Noname manuscript No.
(will be inserted by the editor)

A structure-preserving numerical method for a radially symmetric solution of porous medium equation

Qingqing Zhang · Chenghua Duan · Chun Liu · Cheng Wang · Xingye Yue

Received: date / Accepted: date

Abstract The porous medium equation (PME) is a nonlinear degenerate equation with the finite speed and possible waiting time. Based on an energetic variational approach, a structure-preserving numerical scheme for the one-dimensional PME has been constructed in [12], which preserves the positivity of the solution and the mass conservation, the energy dissipation law, as well as an efficient calculation of the finite speed and the waiting time. In this paper, we use a similar approach to numerically solve a radially symmetric solution of PME in $\mathbb{R}^d$, $d \geq 2$. It is proved that the numerical scheme is uniquely solvable on an admissible convex set and satisfies the original discrete energy dissipation law. Moreover, the optimal rate convergence analysis and error estimate is theoretically established. The two and three dimensional simulation results indicate that the numerical method is effective in solving the axisymmetric solutions of the PME equation, and compute the finite speed and the waiting time effectively. As another advantage, we give the convergence order of the radially symmetric solution with a support and the waiting time numerically in two dimension.

Qingqing Zhang
Department of Mathematics, College of Sciences, Shanghai University, Shanghai 200444, China.
E-mail: zhangqingqing@shu.edu.cn

Chenghua Duan
Department of Mathematics, College of Sciences, Shanghai University, Shanghai 200444, China.
E-mail: chduan@shu.edu.cn

Chun Liu
Department of Applied Mathematics, Illinois Institute of Technology, Chicago, IL 60616, USA.
E-mail: cliu124@iit.edu

Cheng Wang
Department of Mathematics, The University of Massachusetts, North Dartmouth, MA 02747, USA.
E-mail: cwang1@umassd.edu

Xingye Yue
Department of Mathematics and Mathematical Center for Interdiscipline Research, Soochow University, Suzhou 215006, Jiangsu, China.
E-mail: xyyue@suda.edu.cn

Keywords Porous medium equation · energetic variational approach · energy dissipation law · trajectory equation · waiting time

Mathematics Subject Classification (2020) 35K35 · 49J40 · 65M06 · 65M12

1 Introduction

The porous medium equation (PME) is an important class of nonlinear partial differential equations. These equations have important applications in various areas, such as groundwater hydrology, image processing [44], the viscous gravity currents [20], the flow of fluids through porous media [28], etc. The main focus of this research is a radially symmetric solution of porous medium equation:

$$\begin{cases} \partial_t f = \Delta_{\mathbf{x}}(f^m), \mathbf{x} \in \Omega \subset \mathbb{R}^d,\ m > 1,\ t > 0, \\ f(\mathbf{x}, 0) = f_0(\mathbf{x}) \geq 0, \mathbf{x} \in \Omega, \\ \nabla f \cdot \mathbf{n} = 0, \mathbf{x} \in \partial\Omega,\ t > 0, \end{cases} \tag{1.1}$$

where f is a non-negative radially symmetric function, Ω is a bounded domain and $\mathbf{n}$ is the external normal direction, and d stands for the dimension.

Equation (1.1) satisfies the following energy dissipation law

$$\frac{d}{dt}\int_\Omega f(\mathbf{x},t)\ln f(\mathbf{x},t)dx = -\int_\Omega \frac{f(\mathbf{x},t)}{mf(\mathbf{x},t)^{m-1}}|\mathbf{u}|^2\,d\mathbf{x}, \tag{1.2}$$

where $\mathbf{u}$ is the velocity, $\int_\Omega f(\mathbf{x},t)\ln f(\mathbf{x},t)\,dx$ is the total energy and $\int_\Phi \frac{f(\mathbf{x},t)}{mf(\mathbf{x},t)^{m-1}}|\mathbf{u}|^2\,d\mathbf{x}$ is the dissipation term [12].

Since f is a radially symmetric function, the polar coordinates version of equation (1.1) becomes [19]:

$$\begin{cases} \partial_t f = r^{1-d}\dfrac{\partial}{\partial r}\left(r^{d-1}\dfrac{\partial f^m}{\partial r}\right),\ r \in \Omega \subset \mathbb{R}^1,\ m > 1,\ t > 0, \\ f(r,0) = f_0(r) \geq 0,\ r \in \Omega, \\ \nabla f \cdot \mathbf{n}_r = 0,\ r \in \partial\Omega,\ t > 0, \end{cases} \tag{1.3}$$

where $\mathbf{n}_r$ is the external normal direction in the polar coordinates.

The theoretical properties and behaviors of the PME have been extensively studied in many works. The monograph of Vázquez [44] introduces the mathematical theory of the PME. In [3], the regularity properties of flows through porous media are proved. More theoretical analyses are presented in the works by Shmarev [42], Oleĭnik et al. [37], Kalašnikov [26], Barenblatt [4], etc. Furthermore, some issues related to radial symmetry have been studied in many works, such as the local solutions for the exterior domain problem [19], the focusing problem of the radially symmetric PME [2] and the radially symmetric solution of the tempered diffusion equation [1]. Additional research regarding radial symmetry problems could be found in [6,23,22], etc.

Various numerical schemes have been proposed for the PME, such as the finite difference method [21], tracking algorithm [10], and Haar wavelet collocation method

[47]. On the other hand, many classical numerical solutions may contain artificial oscillation, such as moving mesh finite element method [36]. This method is used to handle complex free boundaries, including their emergence and splitting, while the computed solutions exhibiting minor oscillations around these free boundaries. Meanwhile, a local discontinuous Galerkin (LDG) finite element method [48] and variational particle scheme [46] are able to obtain stable numerical solution, eliminating non-physical oscillation in the computational solution near free boundaries. However, there is no theoretical proof regarding the convergence of these numerical methods. Recently, a quarter-sweep finite difference method and the explicit four-points group technique have been proposed in [9]. Numerical experiments have indicated that this method reduces computational complexity while providing an accurate approximation to the porous medium equation. On the other hand, the theoretical analysis of energy dissipation and mass conservation have not been reported.

Based on the energetic variational approach, structure-preserving schemes can be constructed [12]. A remarkable advantage is associated with the fact that the numerical scheme could naturally maintain physical laws such as the mass conservation, energy dissipation, and force balance. Additionally, the waiting time and the finite speed of the free boundary can be effectively computed. A variational Lagrangian scheme for porous medium type generalized diffusion equations was established in [31] via a discrete energetic variational approach, which can capture the free boundary and estimate the waiting time. On the other hand, a rigorous convergence proof was not provided therein. In recent years, neural network-based methods have been applied to solving porous medium equations, such as Physics-Informed Neural Networks (PINNs)[24], a deep JKO scheme[27], a deep minimizing movement scheme[41] and so on. However, when dealing with free boundary evolution, finite speed of propagation and waiting time phenomena, the limited approximation accuracy and the lack of rigorous mathematical convergence proofs constitute the main challenges.

In comparison with the one-dimensional PME by an Energy Variational Approach [12], the mass conservation, energy dissipation law, and trajectory equation for the axisymmetric case should be re-derived. The main challenges in the radially symmetric setting arise from the geometric weight r^{d-1}, especially in terms of its behavior near $r = 0$. For instance, the necessity of imposing a boundary condition at $r = 0$, and the behavior of the solution f involving r^{d-1} at the origin point, need a careful consideration. Furthermore, the convergence analysis must account for the singularity introduced by the geometric weight at $r = 0$.

In this paper, we focus on the structure-preserving numerical method for the radially symmetric solution of PME by an Energy Variational Approach in $\mathbb{R}^d$, $d \geq 2$. Firstly, the original problem is converted from Cartesian to the polar coordinates. Based on the energetic variational approach, the trajectory equation in the polar coordinates could be obtained. Afterward, we construct a numerical scheme, which is uniquely solvable on an admissible convex set and satisfies the corresponding discrete energy dissipation law at a theoretical level. The first order temporal convergence and the second order spatial convergence are proved as well. The computational results demonstrate that the two and three dimensional numerical solutions are stable without oscillation. The free boundary and the waiting time of the radially symmetric could

be effectively computed. Moreover, we are able to obtain the optimal convergence of the solutions with a support and the waiting time numerically.

The organization of this paper is as follows. In Section 2, the trajectory equation for the porous medium equation in the polar coordinate system is derived by the energetic variational approach. In Section 3, the numerical scheme of the trajectory equation is constructed. The theoretical proof of uniqueness, energy stability and optimal rate convergence is provided in Section 4. Finally, some numerical results are presented in Section 5.

2 Energetic Variational Approach

An Energy Variational Approach (EnVarA) was introduced by Onsager [39,40] initially, and was refined and extended by J.W. Strutt [43]. In recent years, it has been widely applied to the mathematical models of the complex fluid [30,25,29] and numerical simulation for nonlinear degenerate equations, including nonlocal Fokker-Planck equation [15], porous medium equation [12]. More details could be found in [12,11, 13,15,33,32,14,16,34].

Based on EnVarA, we derive the trajectory equation for the d-dimensional porous medium equation in the polar coordinates. We first introduce the different coordinate systems.

Definition 2.1 Suppose that $\Omega_0^X, \Omega_t^x \subset \mathbb{R}^d$, $d \in \mathbb{N}^+$, are domains with smooth boundary and time $t > 0$, and $\mathbf{u} = (u_1, ..., u_d)$ is a smooth vector field in $\mathbb{R}^d$. The flow map $x(X,t) : \Omega_0^X \to \Omega_t^x$ is defined as a solution of:

$$\begin{cases} \dfrac{d}{dt}x(X,t) = \mathbf{u}(x(X,t),t), \quad t > 0, \\ x(X,0) = X, \end{cases}$$

where $X = (X_1, ..., X_d) \in \Omega_0^X$ and $x = (x_1, ..., x_d) \in \Omega_t^x$. In turn, the coordinate system X is called the Lagrangian coordinate and the coordinate system x is called Eulerian coordinate [11,14].

Theorem 2.1 *Let $\tilde{F}$ be the Jacobian matrix of the map $X \to x(X,t)$ defined by*

$$\tilde{F}(X,t) := \frac{\partial x(X,t)}{\partial X},$$

which is called the deformation gradient. Then for the radial symmetry in polar coordinates, the determinant of deformation gradient $F(R,t)$ becomes

$$\det F = \frac{r}{R}\frac{\partial r}{\partial R}.$$

Proof We present a detailed proof in the two-dimensional case. Assume the polar coordinates of the reference coordinate (X_1, X_2) and the deformed coordinate (x_1, x_2) are given by (R, Θ) and (r, θ), respectively. In turn, in Lagrangian coordinate, x_1, x_2 become

$$x_1 = r(R,t)\cos\theta, \qquad x_2 = r(R,t)\sin\theta, \qquad r(0,t) = 0,$$

with

$$X_1 = R\cos\Theta, \qquad X_2 = R\sin\Theta, \qquad R(0) = 0.$$

An application of the chain rule yields the computation of the differentials:

$$\begin{aligned} dx_1 &= \cos\theta\, dr - r\sin\theta\, d\theta, \\ dx_2 &= \sin\theta\, dr + r\cos\theta\, d\theta. \end{aligned} \tag{2.1}$$

Meanwhile, the differentials of the reference coordinates turn out to be

$$\begin{aligned} dX_1 &= \cos\Theta\, dR - R\sin\Theta\, d\Theta, \\ dX_2 &= \sin\Theta\, dR + R\cos\Theta\, d\Theta, \end{aligned}$$

i.e.,

$$\begin{aligned} dR &= \cos\theta\, dX_1 + \sin\theta\, dX_2, \\ d\Theta &= -\frac{\sin\theta}{R} dX_1 + \frac{\cos\theta}{R} dX_2. \end{aligned} \tag{2.2}$$

Substituting the radial deformation conditions $dr = (dr/dR)dR$, $\theta = \Theta$ and $d\theta = d\Theta$ into (2.1), we obtain

$$\begin{aligned} dx_1 &= \cos\theta \left(\frac{dr}{dR}\right) dR - r\sin\theta\, d\Theta, \\ dx_2 &= \sin\theta \left(\frac{dr}{dR}\right) dR + r\cos\theta\, d\Theta. \end{aligned} \tag{2.3}$$

With a careful simplification, a substitution of (2.2) into (2.3) leads to

$$\begin{aligned} dx_1 &= \left[\cos^2\theta \left(\frac{dr}{dR}\right) + \frac{r\sin^2\theta}{R}\right] dX_1 + \left[\cos\theta\sin\theta \left(\frac{dr}{dR}\right) - \frac{r\sin\theta\cos\theta}{R}\right] dX_2, \\ dx_2 &= \left[\sin\theta\cos\theta \left(\frac{dr}{dR}\right) - \frac{r\sin\theta\cos\theta}{R}\right] dX_1 + \left[\sin^2\theta \left(\frac{dr}{dR}\right) + \frac{r\cos^2\theta}{R}\right] dX_2. \end{aligned}$$

Therefore, the matrix form of the deformation gradient F becomes

$$F = \begin{pmatrix} \cos^2\theta \left(\frac{dr}{dR}\right) + \frac{r\sin^2\theta}{R} & \cos\theta\sin\theta \left(\frac{dr}{dR}\right) - \frac{r\sin\theta\cos\theta}{R} \\ \sin\theta\cos\theta \left(\frac{dr}{dR}\right) - \frac{r\sin\theta\cos\theta}{R} & \sin^2\theta \left(\frac{dr}{dR}\right) + \frac{r\cos^2\theta}{R} \end{pmatrix}.$$

Introducing the unit vectors $\mathbf{e}_r = (\cos\theta, \sin\theta)$ and $\mathbf{e}_\theta = (-\sin\theta, \cos\theta)$, F could be rewritten as

$$F = \left(\frac{dr}{dR}\right) \mathbf{e}_r \otimes \mathbf{e}_r + \left(\frac{r}{R}\right) \mathbf{e}_\theta \otimes \mathbf{e}_\theta.$$

In the orthogonal basis $\{\mathbf{e}_r, \mathbf{e}_\theta\}$, F is a diagonal matrix with diagonal entries $\frac{dr}{dR}$ and $\frac{r}{R}$; thus its determinant turns out to be

$$\det F = \left(\frac{dr}{dR}\right) \cdot \left(\frac{r}{R}\right) = \frac{r}{R} \frac{\partial r}{\partial R}.$$

This conclusion also holds for the d-dimensional case:

$$\det F = \frac{r^{d-1} \partial_R r}{R^{d-1}}.$$

□

Then we derive the mass conservation law in the polar coordinate.

Theorem 2.2 *In the polar coordinate, mass conservation law becomes*

$$\partial_t f + \frac{1}{r^{d-1}}\partial_r\left(f u_r \cdot r^{d-1}\right) = 0. \tag{2.4}$$

where f is the radially symmetric density function, u_r is the velocity in the r direction and d is the dimension number [5].

The detail proof can be found in [5].

Assume the determinant of deformation gradient $\frac{r^{d-1}\partial_R r}{R^{d-1}} > 0$ in this paper.

Theorem 2.3 *In the Lagrangian coordinate, the mass conservation leads to*

$$f(r(R,t),t) = \frac{f_0(R)R^{d-1}}{r^{d-1}\partial_R r}, \tag{2.5}$$

where $f_0(R)$ is the positive initial data, $\frac{r^{d-1}\partial_R r}{R^{d-1}}$ is the determinant of deformation gradient, assumed to be positive.

Proof We consider the mass contained within any subregion $E_X^0 \subset \Omega_X^0$ given by

$$m_0 = m(0) = \int_{E_X^0} f_0(X)dX.$$

Since the mass is conservative, the mass of any deformed configuration $E_X^t \subset \Omega_X^t$ must be equal to m_0, i.e.,

$$\int_{E_x^t} f(x,t)dx = \int_{E_X^0} f_0(X)dX.$$

Subsequently, the above formula could be converted into a polar coordinate system

$$\int_{E_r^t} f(r,t)r^{d-1}dr = \int_{E_R^0} f(r(R,t),t)r^{d-1}\partial_R r dR = \int_{E_R^0} f_0(R)R^{d-1}dR.$$

Because of the arbitrariness of E_R^0, we see that

$$f(r(R,t),t) = \frac{f_0(R)R^{d-1}}{r^{d-1}\partial_R r}.$$

□

Now we revisit the initial-boundary value problem (1.3) for the porous medium equation, which is equivalent to

$$\partial_t f + \frac{1}{r^{d-1}}\partial_r\left(f u_r \cdot r^{d-1}\right) = 0,\ r \in \Omega_r^t,\ t > 0, \tag{2.6}$$

$$f \cdot u_r = -\partial_r f^m,\ r \in \Omega_r^t,\ t > 0, \tag{2.7}$$

$$f(r,0) = f_0(r) > 0,\ r \in \Omega_r^t, \tag{2.8}$$

$$\nabla f \cdot \mathbf{n}_r = 0,\ r \in \partial\Omega_r^t,\ t > 0, \tag{2.9}$$

where u_r is the radial velocity in the polar coordinate system, and $\mathbf{n}_r$ denotes the unit outward normal vector to the boundary $\partial\Omega_r^t$.

Theorem 2.4 *If $f(r,t)$ is the solution of* (1.3)*, then $f(r,t)$ satisfies the corresponding energy dissipation law*

$$\frac{d}{dt}\int_{\Omega_r^t} f(r,t)\ln f(r,t) r^{d-1} dr = -\int_{\Omega_r^t} \frac{f(r,t)}{m f(r,t)^{m-1}} |u_r|^2 \cdot r^{d-1} dr, \tag{2.10}$$

where u_r is the velocity, d is the dimension number.

Conversely, if $f(r,t)$ satisfies the corresponding energy dissipation law (2.10) *and a zero-flux boundary condition, then $f(r,t)$ is the solution of* (1.3)*.*

The total energy is defined as

$$E^{total} := \int_{\Omega_r^t} f(r,t)\ln f(r,t) r^{d-1} dr,$$

and the dissipation term turns out to be

$$\Delta := \int_{\Omega_r^t} \frac{f(r,t)}{m f(r,t)^{m-1}} |u_r|^2 \cdot r^{d-1} dr.$$

Proof Multiplying both sides of the first equation in (1.3) by $r^{d-1}\ln f + r^{d-1}$, and integrating both sides over Ω_r, we obtain

$$\int_{\Omega_r^t} (r^{d-1}\ln f + r^{d-1})\cdot \partial_t f dr = \int_{\Omega_r^t} (r^{d-1}\ln f + r^{d-1}) \cdot \left(r^{1-d} \frac{\partial}{\partial r}\left(r^{d-1} \frac{\partial f^m}{\partial r} \right) \right) dr.$$

An application of integration by parts gives

$$\int_{\Omega_r^t} (r^{d-1}\ln f + r^{d-1})\cdot \partial_t f dr = -\int_{\Omega_r^t} \frac{\partial f^m}{\partial r} \cdot r^{d-1} d(\ln f + 1) = -\int_{\Omega_r^t} \frac{f}{m f^{m-1}} |u_r|^2 \cdot r^{d-1} dr,$$

where equation (2.7) has been used.

In turn, the following identity becomes valid

$$\frac{d}{dt} E^{total} = -\Delta.$$

Next, we prove that if $f(r,t)$ satisfies the corresponding energy dissipation law (2.10), then $f(r,t)$ is a solution to (1.3) by the energetic variational approach.

– **Least Action Principle**
Based on Least Action Principle, the conservative force could be obtained by taking the variation of the action functional $\mathcal{A}(r)$ with respect to r, where $r(R,t)$ is the flow map.
The action functional is defined as

$$\mathcal{A}(r) := -\int_0^{t^*} \int_{\Omega_R^0} f_0(R) R^{d-1} \ln\left(\frac{f_0(R) R^{d-1}}{r^{d-1}\partial_R r} \right) dR dt,$$

where $t^* > 0$ is a positive number.
Then we obtain the conservation force

$$F_{con} := \frac{\delta \mathcal{A}}{\delta r} = (d-1) f(r,t) r^{d-2} - \partial_r (f(r,t) r^{d-1}) \\ = -\partial_r (f(r,t)) r^{d-1},$$

and

$$F_{con} := (d-1) \frac{f_0(R) R^{d-1}}{r} - \partial_R \left(\frac{f_0(R) R^{d-1}}{\partial_R r} \right),$$

in the Eulerian and Lagrangian coordinates, respectively.

– **Maximum Dissipation Principle**
The Maximum Dissipation Law (Onsager's Principle) means that by taking the variation of $\frac{1}{2}\Delta$ with respect to the velocity u_r, the dissipation force can be obtained [43].
The energy dissipation function is defined as

$$\Delta := \int_{\Omega_r^t} \frac{f(r,t)}{m f(r,t)^{m-1}} |u_r|^2 \cdot r^{d-1} dr,$$

and

$$\Delta := \int_{\Omega_R^0} \frac{f_0(R) R^{d-1}}{m (\frac{f_0(R) R^{d-1}}{r^{d-1} \partial_R r})^{m-1}} \cdot |r_t|^2 dR,$$

in the Eulerian and Lagrangian coordinate systems, respectively, and the dissipation forces turn out to be

$$F_{dis} := \frac{\delta (\frac{1}{2}\Delta)}{\delta u_r} = \frac{f(r,t)}{m f^{m-1}(r,t)} u_r \cdot r^{d-1},$$

$$F_{dis} := \frac{\delta (\frac{1}{2}\Delta)}{\delta \mathbf{r}_t} = \frac{f_0(R) R^{d-1}}{m (\frac{f_0(R) R^{d-1}}{r^{d-1} \partial_R r})^{m-1}} \cdot r_t.$$

– **Force Balance Law**
Based on Newton's force balance law

$$F_{con} = F_{dis},$$

we obtain

$$\frac{f(r,t)}{m f^{m-1}(r,t)} u_r \cdot r^{d-1} = -\partial_r (f(r,t)) r^{d-1}, \tag{2.11}$$

in the Eulerian coordinate., and

$$\frac{f_0(R) R^{d-1}}{m (\frac{f_0(R) R^{d-1}}{r^{d-1} \partial_R r})^{m-1}} \cdot r_t = (d-1) \frac{f_0(R) R^{d-1}}{r} - \partial_R \left(\frac{f_0(R) R^{d-1}}{\partial_R r} \right), \tag{2.12}$$

in the Lagrangian coordinate, which also called as the trajectory equation.

Equation (2.11) is equivalent to (2.7). Therefore, a combination of the boundary conditions (2.8) and (2.9) completes the proof. □

Remark 2.1 In fact, the energy dissipation law in the radial symmetry could be expressed as

$$\frac{d}{dt}\int_{\Omega_r^t}\mathcal{W}(f)r^{d-1}dr = -\int_{\Omega_r^t}\gamma(f)|u_r|^2 r^{d-1}dr,$$

where $\mathcal{W}(f)$ is the density of total energy and $\gamma(f)$ stands for the corresponding dissipation term with the velocity u_r. It suggests that for a given $\mathcal{W}(f)$, there is a corresponding energy dissipation law associated with it. Besides the notation $\mathcal{W}(f) = f\ln f$ used in this paper, alternative forms could be chosen for the porous medium equation, for example

- $\mathcal{W}(f) = \frac{1}{m-1}f^m$, which frequently appears in the porous media equations. The corresponding dissipation term becomes

$$\gamma(f) = f.$$

- $\mathcal{W}(f) = \frac{1}{2f}$, which is often used to describe the elastic energy. Then the corresponding dissipation term is

$$\gamma(f) = \frac{1}{mf^m}.$$

These energy formulations have been discussed in [12]. Based on similar techniques presented in this paper, radially symmetric solutions under different energy formulations could also be obtained. The advantage of entropy choice of $f\ln f$ is that it could naturally guarantee the positivity of the density function.

If the **initial data is positive**, the PME becomes non-degenerate. In this case, the domain $\Omega_r = \Omega_R$, which is noted as Ω uniformly. The initial and boundary conditions for equation (2.12) should be

$$r(R,0) = R,\ R \in \Omega. \tag{2.13}$$

$$r(R,t) = R,\ R \in \partial\Omega,\ t > 0. \tag{2.14}$$

$$r(0,t) = 0,\ t > 0. \tag{2.15}$$

We obtain the trajectory $r(R,t)$ by solving (2.12), (2.13), (2.14) and (2.15), and the solution $f(r,t)$ to the original problem (1.3) by equation (2.5).

Remark 2.2 We observe that the boundary condition (2.15) is reasonable. It is clear that the radially symmetric solution satisfies

$$\partial_r f(r,t)\big|_{r=0} = 0.$$

A substitution of this condition into equation (2.7) gives

$$u_r\big|_{r=0} = -\partial_r f(r,t)\cdot\frac{mf^{m-1}(r,t)}{f(r,t)}\bigg|_{r=0} = 0,$$

which indicates that $r(0,t) = 0$, i.e., equation (2.15) is valid.

Next we provide a justification for the necessity of imposing this boundary condition.

Let $d \geq 2$, $m > 1$. The trajectory equation (2.12) is equivalent to

$$\begin{aligned} r_t =& m\frac{(d-1)}{r}\left(\frac{f_0(R)R^{d-1}}{r^{d-1}\partial_R r}\right)^{m-1} - \frac{m}{f_0(R)R^{d-1}}\left(\frac{f_0(R)R^{d-1}}{r^{d-1}\partial_R r}\right)^{m-1}\frac{\partial_R(f_0(R)R^{d-1})}{\partial_R r} \\ &+ m\left(\frac{f_0(R)R^{d-1}}{r^{d-1}\partial_R r}\right)^{m-1}\frac{\partial_R^2 r}{(\partial_R r)^2} \\ =& m\frac{(d-1)}{r}\left(\frac{f_0(R)R^{d-1}}{r^{d-1}\partial_R r}\right)^{m-1} - \left(\frac{f_0(R)R^{d-1}}{r^{d-1}\partial_R r}\right)^{m-1}\frac{m}{f_0(R)}\frac{\partial_R(f_0(R))}{\partial_R r} \\ &- \left(\frac{f_0(R)R^{d-1}}{r^{d-1}\partial_R r}\right)^{m-1}\frac{m}{\partial_R r}\frac{d-1}{R} + m\left(\frac{f_0(R)R^{d-1}}{r^{d-1}\partial_R r}\right)^{m-1}\frac{\partial_R^2 r}{(\partial_R r)^2},\ R \in \Omega_R^0. \end{aligned}$$

With an application of L'Hôpital's rule, the coefficient of $\partial_R^2 r$ becomes

$$\lim_{R\to 0} m\left(\frac{f_0(R)R^{d-1}}{r^{d-1}\partial_R r}\right)^{m-1}\frac{1}{(\partial_R r)^2} \neq 0.$$

Based on the theory of Fichera-Oleĭnik, the boundary condition (2.15) turns out to be necessary.

If the **initial data has a compact support**, the solution has a free boundary with a finite speed. In the polar coordinates, the right boundary could be defined as

$$\xi^t := \sup\{r \in \Omega : f(r,t) > 0, t \geq 0\}.$$

Let $\Gamma^t := [0, \xi^t] \subset \Omega$.

Hence we solve the initial-boundary value problem is

$$\frac{f_0(R)R^{d-1}}{m\left(\frac{f_0(R)R^{d-1}}{r^{d-1}\partial_R r}\right)^{m-1}}\cdot r_t = (d-1)\frac{f_0(R)R^{d-1}}{r} - \partial_R\left(\frac{f_0(R)R^{d-1}}{\partial_R r}\right),\ R \in \Gamma^0, \tag{2.16}$$

$$(r^{d-1}\partial_R r)^{m-1}\cdot r_t = -\frac{m}{m-1}\frac{\partial_R[f_0(R)R^{d-1}]^{m-1}}{\partial_R r},\ R = \xi^0,\ t > 0, \tag{2.17}$$

$$r(0,t) = 0,\ t > 0, \tag{2.18}$$

$$r(R,0) = R,\ R \in \Gamma^0, \tag{2.19}$$

where the boundary evolution equation (2.17) on the free boundary is derived from equation (2.16) under the condition that $f_0(\xi^0) = 0$.

The detailed derivation is given as follows. The trajectory equation (2.12) is equivalent to

$$\begin{aligned} (r^{d-1}\partial_R r)^{m-1}\cdot r_t =& m(d-1)\frac{m(f_0(R)R^{d-1})^{m-1}}{r} + \frac{m(f_0(R)R^{d-1})^{m-1}\partial_R^2 r}{(\partial_R r)^2} \\ &- \frac{m(f_0(R)R^{d-1})^{m-2}\cdot\partial_R(f_0(R)R^{d-1})\cdot\partial_R r}{(\partial_R r)^2},\ R > 0 \in \Gamma^0,\ t > 0. \end{aligned}$$

Considering $f_0(\xi^0) = 0$, where ξ^0 denotes the right boundary point at time $t = 0$, the first and second terms on the right-hand side of the equation are equal to zero at ξ^0 with $\frac{r^{d-1}\partial_R r}{R^{d-1}} > 0$.

Remark 2.3 The radially symmetric trajectory equations can also be obtained by formulating the higher-dimensional trajectory equations in Cartesian coordinates and then transforming to polar coordinates. Meanwhile, the higher-dimensional formulation inevitably encounters a difficulty, which is the singularity caused by the deformation determinant appearing in the denominator of the trajectory equations. In a direct formulation under axisymmetry, the trajectory equation is one-dimensional, thereby circumventing this issue.

3 The numerical method for the trajectory equation

In this section, we construct the numerical scheme for the trajectory equation.

3.1 Temporal discretization

The trajectory equation (2.12) could be viewed as a gradient flow associated with the total energy

$$E^{total} = \int_{\Omega_R^0} f_0(R) R^{d-1} \ln\left(\frac{f_0(R)R^{d-1}}{r^{d-1}\partial_R r}\right) dR.$$

The Hessian matrix of the total energy E^{total} with respect to $(r, \partial_R r)$ is derived as

$$\begin{pmatrix} (d-1)\frac{f_0(R)R^{d-1}}{r^2} & 0 \\ 0 & \frac{f_0(R)R^{d-1}}{(\partial_R r)^2} \end{pmatrix}.$$

Since the Hessian matrix is a positive definite matrix, E^{total} is a convex function with respect to $r(R,t)$.

To construct an energy stable scheme, the convex splitting methodology [18,11, 7,8,45] could be applied in the temporal discretization. In more details, an implicit approximation is taken if the associated energy is convex. In turn, a *semi-discrete scheme* of equation (2.12) is presented as follows:

$$\frac{f_0(R)R^{d-1}}{m\left(\frac{f_0(R)R^{d-1}}{(r^n)^{d-1}\partial_R r^n}\right)^{m-1}} \cdot \frac{r^{n+1}-r^n}{\tau} = (d-1)\frac{f_0(R)R^{d-1}}{r^{n+1}} - \partial_R\left(\frac{f_0(R)R^{d-1}}{\partial_R r^{n+1}}\right), \quad (3.1)$$

where $\tau := \frac{T}{N}$, $N \in \mathbb{N}^+$, is the time step size, T is the final time, and $r^n = r(R,t^n)$ is the solution at the time step t^n.

Remark 3.1 In fact, the semi-discrete form of the trajectory equation can be expressed as a gradient flow

$$\bar{\gamma}(r^n)\frac{r^{n+1}-r^n}{\tau} = -\frac{\delta \bar{\mathcal{W}}(r^{n+1})}{\delta r^{n+1}},\ n = 0, \cdots, N-1. \quad (3.2)$$

Given r^n for $n = 0, ..., N$, the solution r^{n+1} is the minimizer of the following cost functional:

$$\min_{r^{n+1}\in\Omega}\left\{\int_\Omega \bar{\gamma}(r^n)\frac{\left|r^{n+1}-r^n\right|^2}{2\tau}+\bar{\mathcal{W}}\left(r^{n+1}\right)dR\right\}, \tag{3.3}$$

where $\bar{\mathcal{W}}(r^{n+1})$ is the density of total energy in Lagrangian coordinate at time t^{n+1} and $\bar{\gamma}(r^n)$ stands for the corresponding dissipation term with the velocity r_t at time t^n in Lagrangian coordinate, $n = 0, \cdots, T$.

As noticed in Remark 2.1, the density of total energy $\mathcal{W}(f)$ may have different forms. For each admissible form of $\mathcal{W}(f)$, there exists a corresponding $\gamma(f)$.

- If $\mathcal{W}(f) = f \ln f$, i.e.,

$$\bar{\mathcal{W}}(r^{n+1}) = f_0(R)R^{d-1}\ln\left(\frac{f_0(R)R^{d-1}}{(r^{n+1})^{d-1}\partial_R r^{n+1}}\right),$$

  we have

$$\bar{\gamma}(r^n) = \frac{f_0(R)R^{d-1}}{m\left(\frac{f_0(R)R^{d-1}}{(r^n)^{d-1}\partial_R r^n}\right)^{m-1}}.$$

  The corresponding (3.2) is the trajectory equation (3.1). Due to the presence of the logarithmic function in the energy functional, the solution is naturally positivity-preserving.
- If $\mathcal{W}(f) = \frac{f^m}{m-1}$, i.e.,

$$\bar{\mathcal{W}}(r^{n+1}) = \frac{1}{m-1}\left(\frac{f_0(R)R^{d-1}}{(r^{n+1})^{d-1}\partial_R r^{n+1}}\right)^m,$$

  we have

$$\bar{\gamma}(r^n) = f_0(R)R^{d-1}.$$

  The cost functional (3.3) corresponds to the common Wasserstein gradient-flow formulation of PME with internal energy $\int_\Omega \frac{f^m}{m-1}dx$.

3.2 The fully discrete scheme with a positive initial state

Let R_0 be the first point on the left of Ω and $h = \frac{|\Omega|}{M}$ be the spatial mesh size, with $M \in \mathbb{N}^+$. Denote by $R_i = R_0 + ih$, where i takes on integer and half integer values. Let $\mathcal{E}_M$ and C_M be the spaces of functions, and the domains are given by $\{R_i \mid i = 0, ..., M\}$ and $\{R_{i-\frac{1}{2}} \mid i = 1, ..., M\}$, respectively. In component form, these functions are identified via $l_i = l(R_i)$, $i = 0, ..., M$, for $l \in \mathcal{E}_M$, and $\phi_{i-\frac{1}{2}} = \phi(R_{i-\frac{1}{2}})$, $i = 1, ..., M$, for $\phi \in C_M$.

Let $\mathcal{Q} := \{l \in \mathcal{E}_M \mid l_{i-1} < l_i,\ 1 \le i \le M;\ l_0 = R_0,\ l_M = R_M\}$ be the admissible set, in which the particles are arranged in the order without twisting or exchange. Its boundary set is given by $\partial\mathcal{Q} := \{l \in \mathcal{E}_M \mid l_{i-1} \le l_i,\ 1 \le i \le M,\ and\ l_i = l_{i-1},\ for\ some\ 1 \le i \le M;\ l_0 = R_0,\ l_M = R_M\}$. In turn, $\bar{\mathcal{Q}} := \mathcal{Q} \cup \partial\mathcal{Q}$ is a closed convex set.

The difference operators $D_h : \mathcal{E}_M \to C_M$, $d_h : C_M \to \mathcal{E}_M$, $\widetilde{D}_h : \mathcal{E}_M \to \mathcal{E}_M$, and $\bar{D}_h : \mathcal{E}_M \to \mathcal{E}_M$ are defined as:

$$(D_h l)_{i-\frac{1}{2}} = (l_i - l_{i-1})/h,\ i = 1, ..., M, \tag{3.4}$$

$$(d_h \phi)_i = (\phi_{i+\frac{1}{2}} - \phi_{i-\frac{1}{2}})/h,\ i = 1, ..., M-1, \tag{3.5}$$

$$(\widetilde{D}_h l)_i = \begin{cases} (l_{i+1} - l_{i-1})/2h, & i = 1, \ldots, M-1, \\ (4l_{i+1} - l_{i+2} - 3l_i)/2h,\ i = 0, \\ (l_{i-2} - 4l_{i-1} + 3l_i)/2h,\ i = M. \end{cases} \tag{3.6}$$

$$(\bar{D}_h l)_i = \begin{cases} (l_{i+1} - l_i)/h,\ i = 0, \\ (l_i - l_{i-1})/h,\ i = M. \end{cases} \tag{3.7}$$

– **The positive initial state.** If the initial function is positive in the domain, we solve the initial-boundary value problem (2.12), (2.13), (2.14) and (2.15).
The **fully discrete scheme** is formulated as follows. Given $r^n \in Q$, find $r^{n+1} \in Q$ such that

$$\frac{f_0(R_i)R_i^{d-1}}{m\big(\frac{f_0(R)R^{d-1}}{(r^n)^{d-1}\widetilde{D}_h r^n}\big)_i^{m-1}} \cdot \frac{r_i^{n+1} - r_i^n}{\tau} = (d-1)\Big(\frac{f_0(R)R^{d-1}}{r^{n+1}}\Big)_i - d_h\Big(\frac{f_0(R)R^{d-1}}{D_h r^{n+1}}\Big)_i, \quad \text{for } 1 \le i \le M-1, \tag{3.8}$$

with $r_0^{n+1} = R_0$ and $r_M^{n+1} = R_M$, $n = 0, \ldots, N-1$.

To solve the nonlinear equation (3.8), we use Newton's iteration.
Newton's iteration. Set $r^{n+1,0} = r^n$. For $k = 0, 1, 2, \cdots$, we update $r^{n+1,k+1} = r^{n+1,k} + \delta_r$ such that

$$\frac{f_0(R_i)R_i^{d-1}}{m\big(\frac{f_0(R)R^{d-1}}{(r^n)^{d-1}\widetilde{D}_h r^n}\big)_i^{m-1}} \cdot \frac{\delta_{r_i}}{\tau} + (d-1)\left(\frac{f_0(R)R^{d-1}\delta_{r_i}}{(r^{n+1,k})^2}\right)_i - d_h\left(\frac{f_0(R)R^{d-1}}{(D_h r^{n+1,k})^2} D_h \delta_r\right)_i \tag{3.9}$$
$$= -\frac{f_0(R_i)R_i^{d-1}}{m\big(\frac{f_0(R)R^{d-1}}{(r^n)^{d-1}\widetilde{D}_h r^n}\big)_i^{m-1}} \cdot \frac{r_i^{n+1,k} - r_i^n}{\tau} + (d-1)\left(\frac{f_0(R)R^{d-1}}{r^{n+1,k}}\right)_i - d_h\left(\frac{f_0(R)R^{d-1}}{D_h r^{n+1,k}}\right)_i,$$
for $1 \le i \le M-1$,

with $\delta_{r_0} = \delta_{r_M} = 0$. After the implementation of (3.8), we finally obtain the numerical solution $f_i^n := f(r(R_i, t^n), t^n)$ through the discretization of (2.5), i.e.,

$$f_i^n := \frac{f_0(R_i)R_i^{d-1}}{(r^n)_i^{d-1}(\widetilde{D}_h r^n)_i}. \tag{3.10}$$

– **The initial function with a support.** In this case, the initial-boundary value problem is described by equations (2.16), (2.17), (2.18) and (2.19). We divide the interval Γ^0 into equal subintervals with $R_i = ih$, $i = 0, 1, ..., M$, where M is the number of grid points and the spatial step mesh is $h := (\xi^0 - 0)/M$.

Given the initial state $f_0(R)$ with a compact support Γ^0 and $\{r_i^n\}_{i=0}^M$, find $\{r_i^{n+1}\}_{i=0}^M$ that satisfy the **fully discrete scheme**

$$\frac{f_0(R_i)R_i^{d-1}}{m\big(\frac{f_0(R)R^{d-1}}{(r^n)^{d-1}\bar{D}_h r^n}\big)_i^{m-1}}\frac{r_i^{n+1}-r_i^n}{\tau}=(d-1)\Big(\frac{f_0(R)R^{d-1}}{r^{n+1}}\Big)_i \tag{3.11}$$

$$-d_h\Big(\frac{f_0(R)R^{d-1}}{D_h r^{n+1}}\Big)_i,\ \text{ for }\ 1\le i\le M-1,$$

$$((r^n)_i^{d-1}\bar{D}_h r_i^n)^{m-1}\cdot\frac{r_i^{n+1}-r_i^n}{\tau}=-\frac{m}{m-1}\cdot\frac{\bar{D}_h[f_0(R_i)R_i^{d-1}]^{m-1}}{\bar{D}_h r_i^{n+1}},i=M \tag{3.12}$$

$$\text{with }\ r_0^{n+1}=R_0,\ n=0,\dots,N-1.$$

Since equations (3.11) and (3.12) are nonlinear, we use Newton's iteration (3.9) and

$$\begin{aligned}&((r^n)_i^{d-1}\bar{D}_h r_i^n)^{m-1}\cdot\frac{\delta_{r_i}}{\tau}-\frac{m}{m-1}\cdot\frac{\bar{D}_h[f_0(R_i)R_i^{d-1}]^{m-1}}{(\bar{D}_h r_i^{n+1,k})^2}\bar{D}_h\delta_{r_i}\\&=-((r^n)_i^{d-1}\bar{D}_h r_i^n)^{m-1}\cdot\frac{r_i^{n+1,k}-r_i^n}{\tau}-\frac{m}{m-1}\cdot\frac{\bar{D}_h[f_0(R_i)R_i^{d-1}]^{m-1}}{\bar{D}_h r_i^{n+1,k}},\end{aligned} \tag{3.13}$$

at $i=M$.

4 Theoretical analysis of the numerical scheme

In this section, we provide a theoretical analysis of the numerical scheme (3.8), including the existence and uniqueness, energy stability, the optimal rate of convergence.

Let $l, g\in\mathcal{E}_M$ and $\phi,\varphi\in C_M$. The *inner product* on spaces $\mathcal{E}_M$ and C_M is defined as

$$\langle l,g\rangle:=h\Big(\frac{1}{2}l_0g_0+\sum_{i=1}^{M-1}l_ig_i+\frac{1}{2}l_Mg_M\Big), \tag{4.1}$$

$$\langle\phi,\varphi\rangle_e:=h\sum_{i=0}^{M-1}\phi_{i+\frac{1}{2}}\varphi_{i+\frac{1}{2}}. \tag{4.2}$$

The summation by parts formula is available:

$$\langle l,d_h\phi\rangle=-\langle D_h l,\phi\rangle_e,\ \text{with } l_0=l_M=0,\ \phi\in C_M,\ l\in\mathcal{E}_M. \tag{4.3}$$

First, we prove that there exists a unique solution within the admissible set $\mathcal{Q}$.

Theorem 4.1 *Suppose $f_0(R)\in\mathcal{E}_M$ is positive for $R\in\mathcal{Q}$, then the numerical scheme* (3.8) *is uniquely solvable in $\mathcal{Q}$.*

Proof We first focus on the following optimization problem:

$$\min_{\tilde{r}\in\bar{Q}} J(\tilde{r}) := \frac{1}{2\tau}\Big\langle \frac{f_0(R)R^{d-1}}{m\big(\frac{f_0(R)R^{d-1}}{(r^n)^{d-1}\widetilde{D}_h r^n}\big)^{m-1}}(\tilde{r}-r^n),(\tilde{r}-r^n)\Big\rangle + (d-1)\Big\langle f_0(R)R^{d-1},\ln\Big(\frac{1}{\tilde{r}}\Big)\Big\rangle + \Big\langle f_0(R)R^{d-1},\ln\Big(\frac{f_0(R)R^{d-1}}{D_h\tilde{r}}\Big)\Big\rangle_e, \quad (4.4)$$

where $\tilde{r}\in\bar{Q}$ and $r^n\in Q$ represents the position of particles at time t^n.

A unique minimizer $r\in\bar{Q}$ exists because $J(\tilde{r})$ is a convex function on the closed convex set $\bar{Q}$. Moreover, we must have $r\in Q$, because for any $\tilde{r}\in\partial Q$, there exists some $i>0$ such that $(D_h\tilde{r})_{i-1/2}=(\tilde{r}_i-\tilde{r}_{i-1})/h=0$, resulting in $J(\tilde{r})=+\infty$. Next we aim to prove that $r\in Q$ is the minimizer of $J(\tilde{r})$ if and only if it is a solution of scheme (3.8).

On one hand, assume that $r\in Q$ is the solution to scheme (3.8). We shall prove that r is the minimizer of $J(\tilde{r})$ on $\bar{Q}$.

Since $J(\tilde{r})=+\infty$, we always have $J(\tilde{r})\geq J(r)$, for any $\tilde{r}\in\partial Q$. Then for any $\tilde{r}\in Q$, by taking an inner product with equation (3.8) by $\tilde{r}-r$ and applying summation by parts, we obtain

$$\frac{1}{\tau}\Big\langle \frac{f_0(R)R^{d-1}}{m\big(\frac{f_0(R)R^{d-1}}{(r^n)^{d-1}\widetilde{D}_h r^n}\big)^{m-1}}(r-r^n),\tilde{r}-r\Big\rangle - (d-1)\Big\langle\frac{f_0(R)R^{d-1}}{r},\tilde{r}-r\Big\rangle - \Big\langle\frac{f_0(R)R^{d-1}}{D_h r},D_h(\tilde{r}-r)\Big\rangle_e = 0. \quad (4.5)$$

Subsequently, a direct calculation reveals the following estimate for any $\tilde{r}\in Q$

$$\begin{aligned} J(\tilde{r}) &= J(r+(\tilde{r}-r)) \\ &= J(r)+\frac{1}{2\tau}\Big\langle \frac{f_0(R)R^{d-1}}{m\big(\frac{f_0(R)Rd-1}{(r^n)^{d-1}\widetilde{D}_h r^n}\big)^{m-1}}(\tilde{r}-r),\tilde{r}-r\Big\rangle + \Big\langle f_0(R)R^{d-1},\ln\Big(\frac{D_h r}{D_h\tilde{r}}\Big)\Big\rangle_e \\ &\quad + \frac{1}{\tau}\Big\langle \frac{f_0(R)R^{d-1}}{m\big(\frac{f_0(R)R^{d-1}}{(r^n)^{d-1}\widetilde{D}_h r^n}\big)^{m-1}}(r-r^n),\tilde{r}-r\Big\rangle + (d-1)\Big\langle f_0(R)R^{d-1},\ln\Big(\frac{r}{\tilde{r}}\Big)\Big\rangle \\ &\geq J(r), \end{aligned} \quad (4.6)$$

where the final inequality stems from equation (4.5) and the fact: $\ln\frac{1}{z}\geq -(z-1)$, $\forall z\in\mathbb{R}^+$, which in turn leads to

$$\Big\langle f_0(R)R^{d-1},\ln\Big(\frac{D_h r}{D_h\tilde{r}}\Big)\Big\rangle_e \geq -\Big\langle f_0(R)R^{d-1},\frac{D_h(\tilde{r}-r)}{D_h r}\Big\rangle_e,$$

$$\Big\langle f_0(R)R^{d-1},\ln\Big(\frac{r}{\tilde{r}}\Big)\Big\rangle_e \geq -\Big\langle f_0(R)R^{d-1},\frac{\tilde{r}-r}{r}\Big\rangle.$$

On the other hand, if $r\in Q$ is the minimizer of $J(\tilde{r})$, then for any $\tilde{r}\in\bar{Q}$, since Q is a open convex set, there exists a sufficiently small $\varrho>0$ such that $r+\varrho(\tilde{r}-r)\in Q$.

Then $j(\varrho) := J(r+\varrho(\tilde{r}-r))$ takes its minimum value at $\varrho = 0$. Therefore, we see that $j'(0) = 0$, and an application of summation by parts gives

$$\frac{1}{\tau}\Big\langle \frac{f_0(R)R^{d-1}}{m\big(\frac{f_0(R)R^{d-1}}{(r^n)^{d-1}\widetilde{D}_h r^n}\big)^{m-1}}(r-r^n), \tilde{r}-r\Big\rangle - (d-1)\Big\langle \frac{f_0(R)R^{d-1}}{r^{n+1}}, \tilde{r}-r\Big\rangle$$
$$+\Big\langle d_h\Big(\frac{f_0(R)R^{d-1}}{D_h r^{n+1}}\Big), \tilde{r}-r\Big\rangle = 0,$$

for any $\tilde{r} \in \bar{Q}$. This implies that $r \in Q$ satisfies (3.8). □

Next, we demonstrate that the numerical scheme (3.8) satisfies the corresponding discrete energy dissipation laws.

Theorem 4.2 *Suppose $f_0(R) \in \mathcal{E}_M$ is positive and bounded for $R \in Q$. Let $r^n = (r_0^n, ..., r_M^n) \in Q$ denote the solution to scheme* (3.8) *at time t^n. Then, the discrete energy dissipation law is satisfied:*

$$\frac{E_N(r^{n+1}) - E_N(r^n)}{\tau} \le -\Big\langle \frac{f_0(R)R^{d-1}}{m\big(\frac{f_0(R)R^{d-1}}{(r^n)^{d-1}\widetilde{D}_h r^n}\big)^{m-1}} \frac{r^{n+1}-r^n}{\tau}, \frac{r^{n+1}-r^n}{\tau}\Big\rangle, \tag{4.7}$$

where

$$E_N(r) := \Big\langle f_0(R)R^{d-1}, \ln\Big(\frac{f_0(R)R^{d-1}}{r^{d-1}D_h r}\Big)\Big\rangle_e.$$

Observe that (4.7) represents the discrete version of the energy dissipation laws (2.10).

Proof Because $E_N(x)$ is a convex function, we see that

$$\begin{aligned}\frac{E_N(r^n) - E_N(r^{n+1})}{\tau} &\ge \Big\langle \frac{\delta E_N(r^{n+1})}{\delta r}, \frac{r^n - r^{n+1}}{\tau}\Big\rangle \\ &= \Big\langle -(d-1)\frac{f_0(R)R^{d-1}}{r^{n+1}} + d_h\big(\frac{f_0(R)R^{d-1}}{D_h r^{n+1}}\big), \frac{r^n - r^{n+1}}{\tau}\Big\rangle \\ &= \Big\langle \frac{f_0(R)R^{d-1}}{m\big(\frac{f_0(R)R^{d-1}}{(r^n)^{d-1}\widetilde{D}_h r^n}\big)^{m-1}} \frac{r^n - r^{n+1}}{\tau}, \frac{r^n - r^{n+1}}{\tau}\Big\rangle,\end{aligned} \tag{4.8}$$

where

$$\frac{\delta E_N(r)}{\delta r} = -(d-1)\frac{f_0(R)R^{d-1}}{r} + d_h\Big(\frac{f_0(R)R^{d-1}}{D_h r}\Big).$$

Therefore, (4.7) holds. □

Next, we provide an optimal rate of convergence analysis for the scheme (3.8).

Theorem 4.3 *Assume that $f_0(R)$ is a positive bounded function, r_e is the exact solution of the trajectory equation* (2.12)*, and $r_h \in Q$ is the numerical solution of scheme* (3.9)*, with d the dimension number. Assume that r_e and $partial_R r_e$ have the lower bound, i.e, $\exists \sigma_1$, $\sigma_2 > 0$, s.t. $r_e \geq \sigma_1$ and $\partial_R r_e \geq \sigma_2$. Define the numerical error function as follows*

$$e_i^n = r_{e_i}^n - r_{h_i}^n,\ 0 \leq i \leq M,\ n = 0, \cdots, N. \tag{4.9}$$

Then the following error estimate is available, in the $\ell^\infty(0,T;\ell^2)$ and $\ell^\infty(0,T;H_h^1)$ norms:

$$\|e^n\|_2 := \langle e^n, e^n \rangle \leq C(\tau + h^2),$$

$$\|D_h e^n\|_2 \leq C(\tau + h^2).$$

Moreover, define f_e as the exact solution of the problem (1.3), and f_h as the numerical solution. Then we have

$$\|f_h^n - f_e^n\|_2 \leq C(\tau + h^2),$$

where C is a positive constant, $n = 0, \cdots, N$.

The detailed proof is provided in the appendix.

Remark 4.1 It is assumed that the initial function $f_0(R)$ is positive in the above theoretical analysis. In particular, the positive $f_0(R)$ makes the term $\ln\left(\frac{f_0(R)R^{d-1}}{r^{d-1}D_h r}\right)$ well-defined in the free energy expansion, in Theorems 4.1 and 4.2. In terms of the optimal rate convergence analysis in Theorem 4.3, the exact solution is always sufficiently smooth if the initial data is positive. Using a two-stage error analysis, the first-order temporal convergence and second-order spatial accuracy have been theoretically justified.

However, in the case where the initial data has a compact support, the regularity of the solution will be reduced. Due to the lower order regularity, the functional space for the exact solution is not easy to specify to theoretically justify the convergence analysis, and the current theoretical technique has not been effective to derive an optimal rate error estimate. To better investigate this issue, we compute the convergence order numerically, and demonstrate the variation of the convergence rates, in terms of m, in Section 5.

Remark 4.2 Suppose $f_0(R)$ is a positive bounded function for $R \in Q$. To confirm the convergence of the Newton iteration (3.9) at the theoretical level, we apply the damped Newton iteration to solve the scheme (3.8). The damped Newton iteration could be found in references [11,12,35].

5 Numerical results

In this section, some numerical results are presented. In the first example, we study the solution with a positive bounded function as the initial data to demonstrate the effectiveness of the numerical schemes. The two-dimensional and three-dimensional

Barenblatt solutions are computed in the second and fourth examples, respectively. In the third example, we investigate the waiting time problem. These results verify the advantages of the proposed numerical method in solving free boundary and waiting time phenomena.

The mass conservation in Lagrangian coordinates is given by equation (2.5). When $r = 0$, we use L'Hôpital's Rule to take the limit of equation (2.5), i.e.,

$$f(0,t) = \lim_{R\to 0} \frac{(f_0(R)R^{d-1})'}{(r^{d-1}\partial_R r)'} = \frac{f_0(R)}{(\partial_R r)^d}. \tag{5.1}$$

Therefore, the numerical solution f is obtained by discretizing (2.5) and (5.1) as

$$f_i^n = \frac{f_0(R_i)R_i^{d-1}}{(r^n)_i^{d-1}\widetilde{D}_h r_i^n},\ 1 \le i \le M, \tag{5.2}$$

$$f_i^n = \frac{f_0(R_i)}{(\widetilde{D}_h r_i^n)^d},\ i = 0. \tag{5.3}$$

Example 1. (Positive initial function)

In this example, we solve the problem with a two-dimensional positive initial value:

$$f_0(x,y) = \cos(\frac{\pi}{2}\sqrt{x^2+y^2}) + 0.5,\ \ (x,y) \in \Phi = \left\{(x,y) \mid 0.2 \le x^2+y^2 \le 1\right\}. \tag{5.4}$$

In this example, we apply the fully discrete scheme (3.8) with Newton iteration (3.9) to solve the initial-boundary value problem (2.12), (2.13), (2.14) and (2.15). Finally, the numerical solution is obtained by (5.2) and (5.3). The reference "exact" solution is numerically obtained on a much finer mesh with $h = \frac{1}{100000}$, $\tau = \frac{1}{100000}$.

Tables 1 and 2 present the numerical errors of f, r and the corresponding convergence rates in both the $\mathcal{L}^2$ and $\mathcal{L}^\infty$ norms with a sequence of spatial mesh and time step sizes, $h = \frac{1}{100}, \frac{1}{200}, \frac{1}{400}$ and $\tau = \frac{1}{100}, \frac{1}{400}, \frac{1}{1600}$, at $T = 0.05$ for $m = 3$ and $m = \frac{5}{3}$, respectively. The results demonstrate that the convergence rate of the density f and trajectory r is second order in space and first order in time, for both $m = 3$ and $m = \frac{5}{3}$. Such a full order accuracy comes from the fact that the solution is smooth in this case.

Figure 1 illustrates the evolution of density f for $m = \frac{5}{3}$ at $t = 0$, $t = 0.05$ and $t = 1$. The density f gradually becomes smoother over time until it reaches a steady state. Figure 2 displays the evolution of particle position over time for $R = 0.3$ and $R = 0.5$. It is observed that the particles diffuse outward at a finite speed. Figure 3 describes the total energy decay over time with $h = 1/1000$, $\tau = 1/1000$ for $m = 3$ and $m = \frac{5}{3}$.

Table 1 **Example 1**.The numerical error and convergence order of the numerical solution f and r, with $m = 3$ and $T = 0.05$.

h	τ	$\|e_h^f\|_2$	Order	$\|e_h^f\|_\infty$	Order	$\|e_h^r\|_2$	Order	$\|e_h^r\|_\infty$	Order
1/100	1/100	1.0527e-02		1.8734e-02		2.3064e-03		3.6752e-03	
1/200	1/400	2.7348e-03	1.9446	5.1409e-03	1.8656	5.9474e-04	1.9553	9.5378e-04	1.9461
1/400	1/1600	6.8218e-04	2.0032	1.3077e-03	1.9749	1.4805e-04	2.0062	2.3776e-04	2.0042

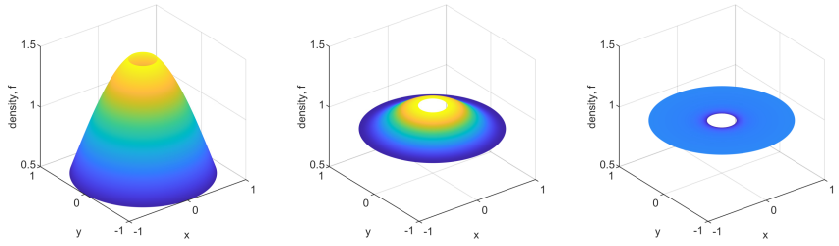

(a) $t = 0$ (b) $t = 0.05$ (c) $t = 1$

Fig. 1 Example 1. The evolution of the numerical density f for $m = \frac{5}{3}$, $h = 1/1000$ and $\tau = 1/1000$ at $t = 0$, $t = 0.05$ and $t = 1$.

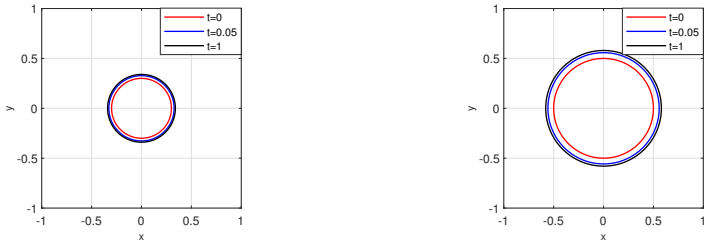

(a) $R = 0.3$ (b) $R = 0.5$

Fig. 2 Example 1. The evolution of particle position at $R = 0.3$, $R = 0.5$ for $m = \frac{5}{3}$, $h = 1/1000$ and $\tau = 1/1000$.

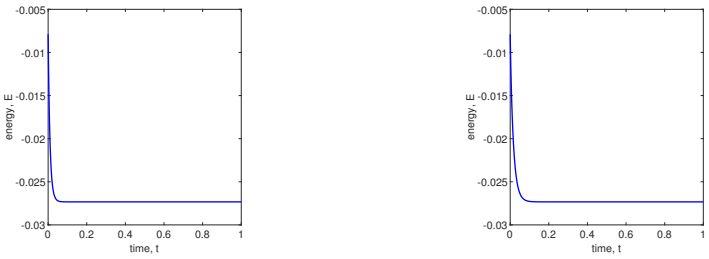

(a) $m = 3$ (b) $m = \frac{5}{3}$

Fig. 3 Example 1. Total energy of positive initial functions over time with $h = 1/1000$, $\tau = 1/1000$ for $m = 3$ and $m = \frac{5}{3}$.

Example 2 (Initial state with a two-dimensional support)

In this example, we solve the 2-D Barenblatt solution, which can be expressed by

$$B_m(x,t) = (t+1)^{-k}\left(1 - \frac{k(m-1)}{4m}\frac{|x|^2}{(t+1)^k}\right)_+^{1/(m-1)}, \; x \in \mathbb{R}^2, \; t \geq 0, \tag{5.5}$$

Table 2 **Example 1**. The numerical error and convergence order of the numerical solution for f and r, with $m = \frac{5}{3}$ and $T = 0.05$.

h	τ	$\|e_h^f\|_2$	Order	$\|e_h^f\|_\infty$	Order	$\|e_h^r\|_2$	Order	$\|e_h^r\|_\infty$	Order
1/100	1/100	1.0380e-02		1.7275e-02		2.2727e-03		3.6467e-03	
1/200	1/400	2.7409e-03	1.9211	4.6964e-03	1.8790	5.9837e-04	1.9253	9.6301e-04	1.9210
1/400	1/1600	6.8717e-04	1.9959	1.1933e-03	1.9766	1.4988e-04	1.9972	2.4131e-04	1.9967

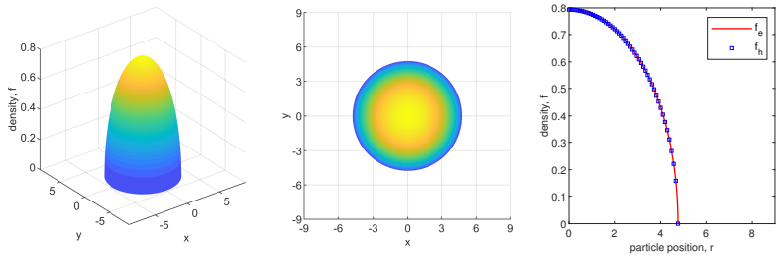

(a) $t = 1$

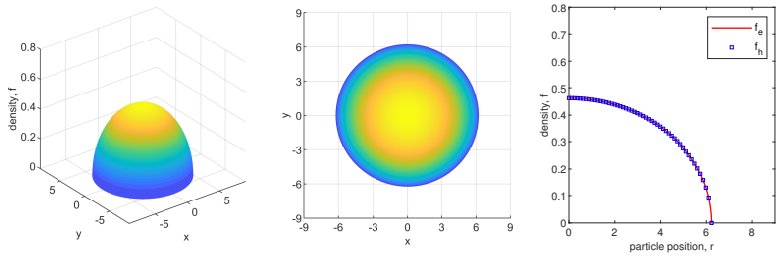

(b) $t = 9$

Fig. 4 **Example 2**. The evolution of the 2-D numerical density f with $m = 3$, $M = 2000$, $\tau = 1/1000$.

with $l_+ = \max\{l, 0\}$ and $k = \frac{1}{m}$. This solution is radially symmetric with a compact support $|x| \le \xi_m^B(t)$, where

$$\xi_m^B(t) := \sqrt{\frac{4m}{k(m-1)}} \cdot (t+1)^{\frac{k}{2}}. \tag{5.6}$$

Define $\Omega = [-9, 9] \times [-9, 9]$. We use $B_m(x, 0)$ as the initial condition for equation (1.1). The fully discrete scheme (3.11) and (3.12) are employed to solve the initial-boundary value problem (2.16), (2.17), (2.18) and (2.19). Newton's iteration is applied, and the numerical solution f is then obtained using formulas (5.2) and (5.3).

Figure 4 illustrates the density f in the polar coordinates at $t = 1$ and $t = 9$ for $m = 3$. From the figure, it is clear that the peak value of the density f decreases over time and the boundary is expanding outward at a finite speed. The numerical solution can effectively approximate the exact solution without oscillation. Figure 5 shows the change in the particle position r over time in the polar coordinates.

Figure 6(a) illustrates the particle boundary at $t = 1$ and $t = 9$ for $m = 3$. The results show that the particle boundary is expanding outward at a finite speed, and the numerical boundary ξ^h is able to approximate the exact boundary ξ^{exact} effectively.

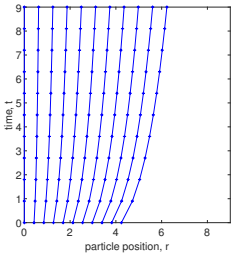

Fig. 5 Example 2. The evolution of the 2-D particle position over time in the polar coordinates for $m = 3$, $M = 2000$ and $\tau = 1/1000$.

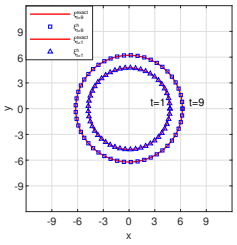

(a) The evolution of boundary over time for $m = 3$.

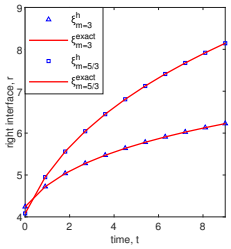

(b) The evolution of right interface for r with $m = 3$ and $m = 5/3$

Fig. 6 Example 2. The evolution of boundary over time ($M = 2000$ and $\tau = 1/1000$).

Figure 6(b) shows the evolution of the right interface over time in the polar coordinates for $m = 3$ and $m = 5/3$.

Table 3 Example 2. The convergence order of f, in the two-dimensional case, for $m = \frac{5}{3}$ and $T = 1$.

M	τ	$\|e_h^f\|_2$	Order	$\|e_h^f\|_\infty$	Order	$e_h^f \, at \, R = 0$	Order
1000	1/250	3.7768e-05		3.4142e-05		3.4142e-05	
2000	1/1000	9.4269e-06	2.0023	8.6943e-06	1.9734	8.6943e-06	1.9734
4000	1/4000	2.3558e-06	2.0005	2.2067e-06	1.9782	2.2067e-06	1.9782

Table 4 Example 2. The convergence order of f, in the two-dimensional case, for $m = 3$ and $T = 1$.

M	τ	$\|e_h^f\|_2$	Order	$\|e_h^f\|_\infty$	Order	$e_h^f \, at \, R = 0$	Order
1000	1/250	5.7496e-04		7.7375e-03		9.6150e-05	
2000	1/1000	2.6316e-04	1.1275	5.1591e-03	0.5848	2.4173e-05	1.9919
4000	1/4000	1.2770e-04	1.0432	3.5705e-03	0.5310	6.0837e-06	1.9904

Tables 3 and 4 present the convergence rate at $T = 1$ for $m = \frac{5}{3}$ and $m = 3$, with a sequence of spatial sizes and time steps ($h = \frac{1}{1000}, \frac{1}{2000}, \frac{1}{4000}$ and $\tau = \frac{1}{250}, \frac{1}{1000}, \frac{1}{4000}$), respectively. When $m = \frac{5}{3}$, the spatial convergence order of the numerical solution f

is second-order in both the $\mathcal{L}^2$ and $\mathcal{L}^\infty$ norms. However, when $m = 3$, the $\mathcal{L}^2$ and $\mathcal{L}^\infty$ convergence order of f decreases to 1 and $\frac{1}{2}$, respectively. The reason is that the regularity of solution decreases as m increases near the boundary. Since $R = 0$ is an interior point, f remains smooth away from the boundary.

Example 3 (Waiting time phenomenon)

In the polar coordinate system, the trajectory equation of the right interface becomes

$$\partial_t r = -\frac{m}{m-1}\frac{\partial_R[f_0(R)R^{d-1}]^{m-1}}{(r^{d-1})^{m-1}(\partial_R r)^m},\ R = \xi^0,\ t > 0. \tag{5.7}$$

Let

$$\mathcal{B}_h^n := \frac{\bar{D}_h[(f_0(R_0)R_0^{d-1})^{m-1}]}{((r_{h,0}^n)^{d-1})^{m-1}(\bar{D}_h r_{h,0}^n)^m},$$

where $r_h^n = (r_{h,0}^n, \cdots, r_{h,M}^n)$ is the numerical trajectory position at time t^n, $n = 0, \cdots, N$. The numerical waiting time t_h^* is determined by the following criterion [15, 12]:

$$t_h^* := \min\left\{t^n : \left|\frac{\mathcal{B}_{2h}^n}{\mathcal{B}_h^n}\right| \le 1\right\}. \tag{5.8}$$

To get $\mathcal{B}_{2h}^n$ in the above formula, the trajectory r_{2h}^n is selected from the given solution r_h^n, i.e., $r_{2h}^n = (r_{h,0}^n, r_{h,2}^n, r_{h,4}^n, \cdots)$.

Next, we consider the waiting time of two-dimensional problem (1.1).

Let $\Omega = [-2.5, 2.5] \times [-2.5, 2.5]$, and

$$D := \left\{(x, y) \mid x^2 + y^2 \le \left(\frac{\pi}{2}\right)^2\right\} \subseteq \Omega,$$

$$f_0(x, y) = \begin{cases} \left\{\frac{m-1}{m}\left[\frac{3}{4}\cos^2\sqrt{x^2+y^2} + \frac{1}{4}\cos^4\sqrt{x^2+y^2}\right]\right\}^{1/(m-1)}, & (x, y) \in D, \\ 0, & \text{otherwise in } \Omega. \end{cases} \tag{5.9}$$

The fully discrete scheme (3.8), combined with Newton's iteration solver (3.9), is used to obtain the numerical solution r^n. Then we check whether r^n meets the waiting time criterion (5.8). If the criterion is satisfied, the waiting time is determined as $t_h^* = t^n$; otherwise, we proceed to the next time step. After the waiting time, we use the corresponding Newton iteration of scheme (3.11) and (3.12) to solve the problem.

Figure 7 depicts the density f before and after the waiting time in the polar coordinate system for $m = 3$, $M = 2000$ and $\tau = 1/2000$. The numerical waiting time is determined as $t_h^* = 0.1700$. After this time, the boundary interface begins to move outward at a finite speed. Figure 8 shows the changes of particle domain before and after the waiting time from a top view perspective. Table 5 presents the convergence order of the waiting time for $m = 3$. The refines waiting time is calculated using $M = 10000$ and $\tau = 1/10000$. Therefore, the convergence order of the waiting time is numerically estimated to be at least $\frac{1}{2}$.

Example 4 (Initial function with a three-dimensional support)

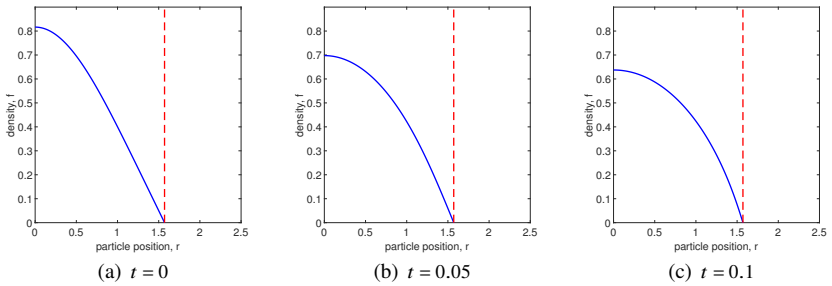

(a) $t = 0$ (b) $t = 0.05$ (c) $t = 0.1$

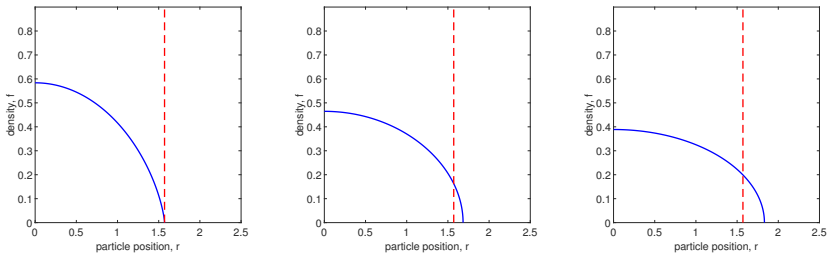

(d) $t = 0.1700$ (e) $t = 0.5$ (f) $t = 1$

Fig. 7 Example 3. Waiting time: Evolution of f in the polar coordinates ($m = 3$, $M = 2000$, $\tau = 1/2000$).

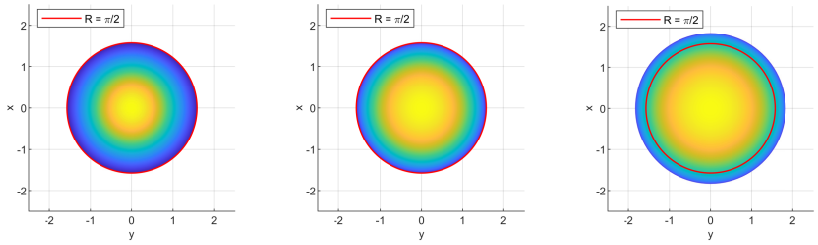

(a) $t = 0$ (b) $t = 0.17$ (c) $t = 1$

Fig. 8 Example 3. The top view of the development of solution f ($m = 3$, $M = 2000$, $\tau = 1/2000$).

The three-dimensional Barenblatt-Pattle solution is given by

$$B_m(x,t) = (t+1)^{-k}\Big(1 - \frac{k(m-1)}{6m}\frac{|x|^2}{(t+1)^{2k/3}}\Big)_+^{1/(m-1)}, \; x \in \mathbb{R}^d, \; d = 3, \; t \geq 0, \quad (5.10)$$

where $l_+ = \max\{l, 0\}$ and $k = (m - 1 + 2/d)^{-1}$. This solution has compact support $|x| \leq \xi_m^B(t)$, where

$$\xi_m^B(t) := \sqrt{\frac{6m}{k(m-1)}} \cdot (t+1)^{\frac{k}{d}}. \quad (5.11)$$

We use $B_m(x,0)$ as the initial data for equation (1.1) on $\Omega = [-8,8]^3$. The fully discrete scheme (3.11) and (3.12) is employed to solve the initial-boundary value

Table 5 **Example 3**. The convergence rate of waiting time with $m = 3$

M	τ	t_w^*	$\lvert t_w^* - t_{w,e}^* \rvert$	Order
100	1/100	0.19	0.0219	
200	1/200	0.180	0.0119	0.8800
400	1/400	0.1750	0.0069	0.7863
800	1/800	0.1725	0.0044	0.6491
$t_{w,e}^*$		0.1681		

1. t_w^* is the numerical wait time and $t_{w,e}^*$ is the exact waiting time.

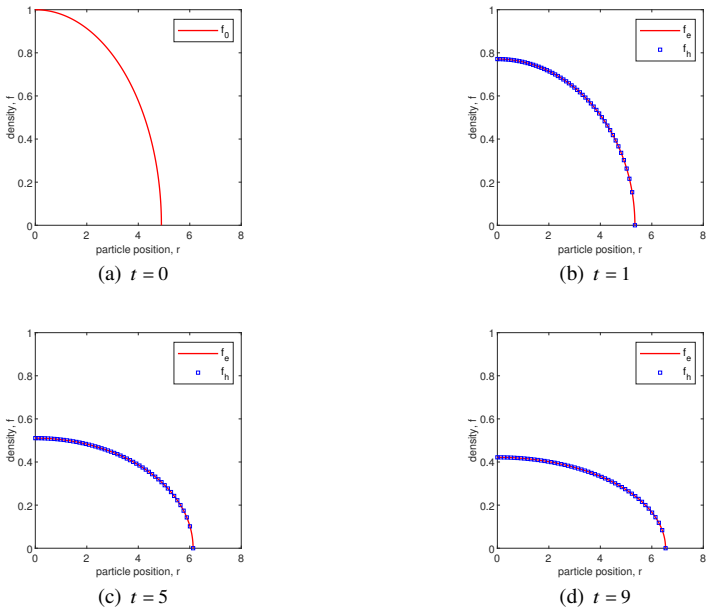

(a) $t = 0$ (b) $t = 1$

(c) $t = 5$ (d) $t = 9$

Fig. 9 **Example 4**. The evolution of the 3D numerical density f in the polar coordinates ($m = 3$, $M = 2000$ and $\tau = 1/1000$).

problem (2.16), (2.17), (2.18) and (2.19). Figure 9 illustrates the evolution of the numerical density and the exact solution in the polar coordinate system for $m = 3$. The results indicate that the numerical solution can approximate the exact solution effectively. Figure 10 depicts the evolution of the domain over time at a finite speed. Table 6 displays the convergence order of three-dimensional f for $m = 3$ and $T = 1$, which is first order in $\mathcal{L}^2$ norm, $\frac{1}{2}$ order in $\mathcal{L}^\infty$, and second order at $R = 0$.

Table 6 **Example 4**. The convergence order of three-dimensional f for $m = 3$ and $T = 1$.

M	τ	$\lVert e_h^f \rVert_2$	Order	$\lVert e_h^f \rVert_\infty$	Order	e_h^f at $R = 0$	Order
1000	1/250	5.9543e-04		7.2877e-03		1.3747e-04	
2000	1/1000	2.6820e-04	1.1506	4.9064e-03	0.5708	3.4648e-05	1.9883
4000	1/4000	1.2995E-04	1.0453	3.4185E-03	0.5213	8.7291E-06	1.9888

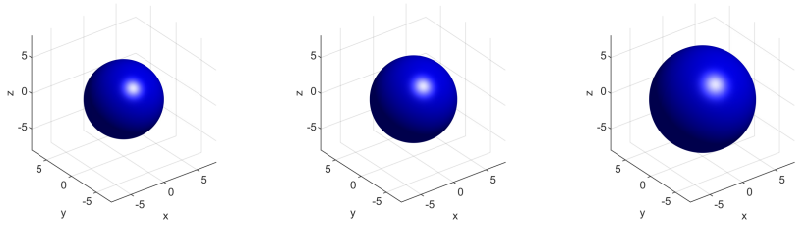

(a) $t = 0$ (b) $t = 1$ (c) $t = 9$

Fig. 10 Example 4. The evolution of the 3-D boundary over time ($m = 3$, $M = 2000$ and $\tau = 1/1000$).

6 Conclusions

In this paper, we have proposed and analyzed a numerical scheme for a radially symmetric solution of the porous medium equation using an energetic variational method. The unique solvability of this numerical method on an admissible convex set is proven, and the numerical scheme satisfies a discrete energy dissipation law. Moreover, the optimal convergence analysis and error estimate is established. The numerical results are able to approximate the exact solution without oscillation, and the waiting time has been effectively computed.

On the other hand, the limitation of this work is associated with the radial symmetry of the density f in the porous medium equation. For more general cases will be considered in our future work.

Acknowledgments. Chenghua Duan was supported in part by NSFC 11901109. The work of Chun Liu is partially supported by NSF grants DMS-1950868 and DMS-2118181. The work of Cheng Wang is partially supported by NSF grants DMS-2012269 and DMS-2309548. The work of Xingye Yue was supported by NSFC 12371401.

Appendix: Proof of Theorem 4.3

In this appendix, we give a detail proof of Theorem 4.3 for the numerical scheme (3.8). First, we introduce a higher-order approximate expansion of the exact solution.

Lemma 6.1 *Suppose a higher order approximate solution of the exact solution r_e takes the form of*

$$W := r_e + \tau w_\tau^{(1)} + \tau^2 w_\tau^{(2)} + h^2 w_h, \tag{6.1}$$

where $w_\tau^{(1)}$, $w_\tau^{(2)}$, $w_h \in C^\infty(\Omega; [0,T])$. Then there exists a sufficiently small $\tau_0 > 0$, such that $\forall \tau, h \le \tau_0$, we have $\widetilde{D}_h W > 0$, i.e., $W \in \mathcal{Q}$, where τ and h are the time step and the spatial mesh sizes, respectively.[13]

Then we proceed with the proof of Theorem 4.3.

Proof of Theorem 4.3:

Proof For $2 \le i \le M-1$, a detailed Taylor expansion of the fully discrete scheme gives

$$\begin{aligned}
&\frac{f_0(R_i)R_i^{d-1}}{m\left(\frac{f_0(R)R^{d-1}}{(r_e^n)^{d-1}\widetilde{D}_h r_e^n}\right)_i^{m-1}}\cdot\frac{r_{e_i}^{n+1}-r_{e_i}^n}{\tau} \\
&=(d-1)\left(\frac{f_0(R)R^{d-1}}{r_e^{n+1}}\right)_i-d_h\left(\frac{f_0(R)R^{d-1}}{D_h r_e^{n+1}}\right)_i+\tau l_i^{(1)}+\tau^2 l_i^{(2)}+\tau^3 l_i^{(3)}+h^2 g_i^{(1)}+h^4 g_i^{(2)}, \\
&\text{with } r_{e_0}^{n+1}=R_0,\ \ r_{e_M}^{n+1}=R_M,
\end{aligned} \tag{6.2}$$

where $\|l^{(1)}\|_2, \|l^{(2)}\|_2, \|l^{(3)}\|_2, \|g^{(1)}\|_2, \|g^{(2)}\|_2 \le C_e$, and C_e relies only on the exact solution.

The constructed approximation $W \in Q$ satisfies the following numerical scheme with higher-order truncation error:

$$\begin{aligned}
&\frac{f_0(R_i)R_i^{d-1}}{m\left(\frac{f_0(R)R^{d-1}}{(W^n)^{d-1}\widetilde{D}_h W^n}\right)_i^{m-1}}\cdot\frac{W_i^{n+1}-W_i^n}{\tau} \\
&=(d-1)\left(\frac{f_0(R)R^{d-1}}{W^{n+1}}\right)_i-d_h\left(\frac{f_0(R)R^{d-1}}{D_h W^{n+1}}\right)_i+\tau^3 l_i^*+h^4 g_i^*,\ \ 2\le i\le M-1, \\
&\text{with } W_0^{n+1}=R_0,\ \ W_M^{n+1}=R_M,\ \ n=0,1,\cdots,N-1,
\end{aligned}$$

where l^*, g^* are determined by $l^{(1)}$, $l^{(2)}$, $l^{(3)}$, $g^{(1)}$, $g^{(2)}$ and $w_\tau^{(1)}$, $w_\tau^{(2)}$, w_h.

In fact, the expansion term $w_\tau^{(1)} \in C^\infty(\Omega;0,T)$ satisfies the following equation:

$$\begin{aligned}
&\frac{f_0(R)R^{d-1}}{m\left(\frac{f_0(R)R^{d-1}}{r_e^{d-1}\partial_R r_e}\right)^{m-1}}\partial_t w_\tau^{(1)}+\frac{(m-1)\partial_t r_e}{m(\frac{f_0(R)R^{d-1}}{r_e^{d-1}\partial_R r_e})^{m-2}}((d-1)r_e^{d-2}\partial_R r_e\cdot w_\tau^{(1)}+r_e^{d-1}\cdot\partial_R w_\tau^{(1)}) \\
&=-(d-1)\left(\frac{f_0(R)R^{d-1}}{r_e^2}\right)w_\tau^{(1)}+\partial_R\left(\frac{f_0(R)R^{d-1}}{(\partial_R r_e)^2}\partial_R w_\tau^{(1)}\right)-l^{(1)}, \\
&w_\tau^{(1)}|_{\partial\Omega}=0,\quad w_\tau^{(1)}(\cdot,0)=0.
\end{aligned} \tag{6.3}$$

The term $w_\tau^{(2)} \in C^\infty(\Omega;0,T)$ satisfies the following equation:

$$
\begin{aligned}
&\frac{f_0(R)R^{d-1}}{m\left(\frac{f_0(R)R^{d-1}}{r_e^{d-1}\partial_R r_e}\right)^{m-1}}\partial_t w_\tau^{(2)} + \frac{(m-1)\partial_t r_e}{m(\frac{f_0(R)R^{d-1}}{r_e^{d-1}\partial_R r_e})^{m-2}}((d-1)r_e^{d-2}\partial_R r_e \cdot w_\tau^{(2)} + r_e^{d-1}\cdot\partial_R w_\tau^{(2)})\\
&+\frac{(m-1)\partial_t w_\tau^{(1)}}{m(\frac{f_0(R)R^{d-1}}{r_e^{d-1}\partial_R r_e})^{m-2}}((d-1)r_e^{d-2}\partial_R r_e \cdot w_\tau^{(1)} + r_e^{d-1}\cdot\partial_R w_\tau^{(1)})\\
&+(w_\tau^{(1)})^2\frac{(m-1)(d-1)r_e^{d-3}\partial_R r_e[(m-2)(d-1)+(d-2)]}{2m\left(\frac{f_0(R)R^{d-1}}{r_e^{d-1}\partial_R r_e}\right)^{m-2}}\partial_t r_e\\
&+(\partial_R w_\tau^{(1)})^2\frac{(m-1)(m-2)\partial_t r_e}{2m\left(\frac{f_0(R)R^{d-1}}{r_e^{d-1}\partial_R r_e}\right)^{m-2}r_e^{d-1}\partial_R r_e}(r_e^{d-1})^2 + w_\tau^{(1)}\partial_R w_\tau^{(1)}\frac{(m-1)^2(d-1)r_e^{d-2}}{m\left(\frac{f_0(R)R^{d-1}}{r_e^{d-1}\partial_R r_e}\right)^{m-2}}\partial_t r_e\\
&=-(d-1)\frac{f_0(R)R^{d-1}}{r_e^2}w_\tau^{(2)} + \partial_R\Big(\frac{f_0(R)R^{d-1}}{(\partial_R r_e)^2}\partial_R w_\tau^{(2)}\Big)\\
&+(d-1)\frac{f_0(R)R^{d-1}}{r_e^3}(w_\tau^{(1)})^2 - \partial_R\Big(\frac{f_0(R)R^{d-1}}{(\partial_R r_e)^3}(\partial_R w_\tau^{(1)})^2\Big) - l^{(2)},\\
&w_\tau^{(2)}|_{\partial\Omega}=0, \quad w_\tau^{(2)}(\cdot,0)=0.
\end{aligned}
\tag{6.4}
$$

The term $w_h \in C^\infty(\Omega;0,T)$ satisfies the following equation:

$$
\begin{aligned}
&\frac{f_0(R)R^{d-1}}{m\left(\frac{f_0(R)R^{d-1}}{r_e^{d-1}\partial_R r_e}\right)^{m-1}}\partial_t w_h + \frac{(m-1)\partial_t r_e}{m(\frac{f_0(R)R^{d-1}}{r_e^{d-1}\partial_R r_e})^{m-2}}((d-1)r_e^{d-2}\partial_R r_e \cdot w_h + r_e^{d-1}\cdot\partial_R w_h)\\
&=-(d-1)\left(\frac{f_0(R)R^{d-1}}{r_e^2}\right)w_h + \partial_R\Big(\frac{f_0(R)R^{d-1}}{(\partial_R r_e)^2}\partial_R w_h\Big) - g^{(1)},\\
&w_h|_{\partial\Omega}=0, \quad w_h(\cdot,0)=0.
\end{aligned}
\tag{6.5}
$$

Based on the fact that $w_\tau^{(1)}$, $w_\tau^{(2)}$, w_h are determined solely by W and r_e, we see that

$$\|W-r_e\|_{H^m} = \tau\|w_\tau^{(1)}\|_{H^m} + \tau^2\|w_\tau^{(2)}\|_{H^m} + h^2\|w_h\|_{H^m} \le C'(\tau+h^2).$$

Define $\tilde{e}_i^n := W_i^n - r_{h_i}^n$, $0 \le i \le M$, $n = 0,1,\cdots,N$. In other word, we evaluate the numerical error between the numerical solution and the constructed solution W, rather than performing a direct comparison between the numerical solution and the exact solution. Next, we focus on the interior grid points, where $2 \le i \le M-1$. Notice that $\|\tilde{e}^0\|_2 = 0$ at time step t^0. The following a-priori assumption is made at the previous time step t^n:

$$\|\tilde{e}^n\|_2 \le (\tau^{\frac{11}{4}} + h^{\frac{7}{2}}). \tag{6.6}$$

Based on the priori assumption, the following estimates become available:

$$\|D_h\tilde{e}^n\|_2 \le C(\tau^{\frac{7}{4}}+h^{\frac{5}{2}}), \tag{6.7}$$

$$\|D_h\tilde{e}^n\|_\infty \le C_m\frac{\|D_h\tilde{e}^n\|_2}{h^{1/2}} \le CC_m(\tau^{\frac{5}{4}}+h^2),\ \text{if}\ \ h=O(\tau), \tag{6.8}$$

$$\|D_h r_h^n\|_\infty = \|D_h W^n - D_h\tilde{e}^n\|_\infty \le C^*+1 := C_0^*, \tag{6.9}$$

$$\text{with}\ \ C^* := \|D_h W^n\|_\infty,\ \ \text{if}\ \ CC_m(\tau^{\frac{5}{4}}+h^2)\le 1,$$

$$\|\tilde{e}^n\|_\infty \le C_m\frac{\|\tilde{e}^n\|_2}{h^{1/2}} \le C_m(\tau^{\frac{9}{4}}+h^3),\ \text{if}\ \ h=O(\tau), \tag{6.10}$$

$$\|r_h^n\|_\infty = \|W^n-\tilde{e}^n\|_\infty \le C_r+1 := C_r^*,\ \text{if}\ \ C_m(\tau^{\frac{9}{4}}+h^3)\le 1, \tag{6.11}$$

$$\left\|\frac{r_h^n-r_h^{n-1}}{\tau}\right\|_\infty = \left\|\frac{W^n-W^{n-1}}{\tau}-\frac{\tilde{e}^n-\tilde{e}^{n-1}}{\tau}\right\|_\infty \le C_t^*+1, \tag{6.12}$$

$$\text{with}\ \ C_t^* := \left\|\frac{W^n-W^{n-1}}{\tau}\right\|_\infty,\ \text{if}\ \ C_m(\tau^{\frac{5}{4}}+h^2)\le 1,$$

$$\left\|\frac{D_h r_h^n-D_h r_h^{n-1}}{\tau}\right\|_\infty = \left\|\frac{D_h W^n-D_h W^{n-1}}{\tau}-\frac{D_h\tilde{e}^n-D_h\tilde{e}^{n-1}}{\tau}\right\|_\infty \le \tilde{C}_t^*+1, \tag{6.13}$$

$$\text{with}\ \ \tilde{C}_t^* := \left\|\frac{D_h W^n-D_h W^{n-1}}{\tau}\right\|_\infty,\ \text{if}\ \ CC_m(\tau^{\frac{1}{4}}+h)\le 1.$$

Since $r_h, W\in Q$, i.e., $\exists\,\sigma_2>0$, such that $D_h W_i^n \ge 2\sigma_2$, then $D_h r_{h_i}^n \ge \sigma_2 > 0, 0\le i\le M$, if $CC_m(\tau^{\frac{5}{4}}+h^2)\le\sigma_2$.

Next, a subtraction of (6.3) from the numerical scheme (3.8) results in

$$\begin{aligned}
&\frac{f_0(R_i)R_i^{d-1}}{m\left(\frac{f_0(R)R^{d-1}}{(r_h^n)^{d-1}\widetilde{D}_h r_h^n}\right)_i^{m-1}}\cdot\frac{\tilde{e}_i^{n+1}-\tilde{e}_i^n}{\tau} \\
&+\frac{f_0(R_i)R_i^{d-1}}{m[f_0(R_i)R_i^{d-1}]^{m-1}}\cdot\frac{W_i^{n+1}-W_i^n}{\tau}\cdot\left[\left((W^n)^{d-1}\widetilde{D}_h W^n\right)_i^{m-1}-\left((r_h^n)^{d-1}\widetilde{D}_h r_h^n\right)_i^{m-1}\right] \\
&=-(d-1)\left(\frac{f_0(R)R^{d-1}}{W^{n+1}r_h^{n+1}}\right)_i\tilde{e}_i^{n+1}+d_h\left(\frac{f_0(R)R^{d-1}}{D_h W^{n+1}D_h r_h^{n+1}}D_h\tilde{e}^{n+1}\right)_i+\tau^3 l_i^*+h^4 g_i^*, \\
&\text{for}\ 2\le i\le M-1,\ \text{with}\ \tilde{e}_0^{n+1}=\tilde{e}_M^{n+1}=0.
\end{aligned} \tag{6.14}$$

Taking a discrete inner product with (6.14) by $2\tilde{e}^{n+1}$ yields

$$\begin{aligned}
&2\left\langle\alpha_n(\tilde{e}^{n+1}-\tilde{e}^n),\tilde{e}^{n+1}\right\rangle-2\tau\left\langle d_h\left(\frac{f_0(R)R^{d-1}}{D_h W^{n+1}D_h r_h^{n+1}}D_h\tilde{e}^{n+1}\right),\tilde{e}^{n+1}\right\rangle \\
&=-2\tau\left\langle\frac{f_0(R)R^{d-1}}{m[f_0(R)R^{d-1}]^{m-1}}\frac{W^{n+1}-W^n}{\tau}[((W^n)^{d-1}\widetilde{D}_h W^n)^{m-1}-((r_h^n)^{d-1}\widetilde{D}_h r_h^n)^{m-1}],\tilde{e}^{n+1}\right\rangle \\
&\quad-2\tau\left\langle(d-1)\frac{f_0(R)R^{d-1}}{W^{n+1}r_h^{n+1}}\tilde{e}^{n+1},\tilde{e}^{n+1}\right\rangle+2\tau\left\langle\tau^3 l^*+h^4 g^*,\tilde{e}^{n+1}\right\rangle,
\end{aligned} \tag{6.15}$$

where

$$\alpha_n := \frac{f_0(R)R^{d-1}}{m\left(\frac{f_0(R)R^{d-1}}{(r_h^n)^{d-1}\widetilde{D}_h r_h^n}\right)^{m-1}}.$$

With the assumption that $0 < b_f \le f_0(R)R^{d-1} \le B_f$, α_n has the lower and upper bounds:

$$C_\alpha := \frac{b_f}{m(\frac{B_f}{(\sigma_1)^{d-1}\sigma_2})^{m-1}} \le \|\alpha_n\|_\infty \le \frac{B_f}{mb_f^{m-1}}((C_r^*)^{d-1}C_0^*)^{m-1} := \bar{C}_\alpha.$$

The first term on the left-hand side could be analyzed as follows:

$$\begin{aligned} 2\left\langle \alpha_n(\tilde{e}^{n+1}-\tilde{e}^n), \tilde{e}^{n+1}\right\rangle &= \alpha_n\|\tilde{e}^{n+1}\|_2^2 + \alpha_n\|\tilde{e}^{n+1}-\tilde{e}^n\|_2^2 - \alpha_n\|\tilde{e}^n\|_2^2 \\ &\ge \alpha_n\|\tilde{e}^{n+1}\|_2^2 - \alpha_n\|\tilde{e}^n\|_2^2. \end{aligned} \tag{6.16}$$

Regarding the second term on the left-hand side, it is evident that

$$\begin{aligned} &-2\tau\left\langle d_h\left(\frac{f_0(R)R^{d-1}}{D_hW^{n+1}D_hr_h^{n+1}}D_h\tilde{e}^{n+1}\right), \tilde{e}^{n+1}\right\rangle \\ &= 2\tau\left\langle \frac{f_0(R)R^{d-1}}{D_hW^{n+1}D_hr_h^{n+1}}D_h\tilde{e}^{n+1}, D_h\tilde{e}^{n+1}\right\rangle_e \ge 0, \end{aligned} \tag{6.17}$$

based on the summation by parts formula, combined with the boundary condition

$$\tilde{e}_0^{n+1} = \tilde{e}_N^{n+1} = 0.$$

The first term on the right-hand side could be bounded by

$$\begin{aligned} &-2\tau\left\langle \frac{f_0(R)R^{d-1}}{m[f_0(R)R^{d-1}]^{m-1}}\frac{W^{n+1}-W^n}{\tau}[\left((W^n)^{d-1}\widetilde{D}_hW^n\right)^{m-1} - \left((r_h^n)^{d-1}\widetilde{D}_hr_h^n\right)^{m-1}], \tilde{e}^{n+1}\right\rangle \\ &= -2\tau\left\langle \frac{f_0(R)R^{d-1}}{m[f_0(R)R^{d-1}]^{m-1}}\cdot\frac{W^{n+1}-W^n}{\tau}\cdot(V_1\tilde{e}^n + V_2\widetilde{D}_h\tilde{e}^n), \tilde{e}^{n+1}\right\rangle \\ &\le 2\tau C_1\|\tilde{e}^n\|_2\|\tilde{e}^{n+1}\|_2 + 2\tau C_2\|\widetilde{D}_h\tilde{e}^n\|_2\|\tilde{e}^{n+1}\|_2, \quad \left(C_1 := \frac{B_fC_t^*C_\zeta^1}{mb_f^{(m-1)}},\ C_2 := \frac{B_fC_t^*C_\zeta^2}{mb_f^{(m-1)}}\right) \\ &\le \tau C_1\|\tilde{e}^n\|_2^2 + \tau C_1\|\tilde{e}^{n+1}\|_2^2 + \tau C_2\|\widetilde{D}_h\tilde{e}^n\|_2^2 + \tau C_2\|\tilde{e}^{n+1}\|_2^2, \end{aligned} \tag{6.18}$$

where $C_t^* = \|W_t\|_\infty$, ζ is between r_h^n and W^n, and

$$\|V_1\|_\infty = \|(m-1)((\zeta^n)^{d-1}\widetilde{D}_h\zeta^n)^{m-2}(d-1)(\zeta^n)^{d-2}\widetilde{D}_h\zeta^n\|_\infty \le C_\zeta^1,$$

$$\|V_2\|_\infty = \|(m-1)((\zeta^n)^{d-1}\widetilde{D}_h\zeta^n)^{m-2}(\zeta^n)^{d-1}\|_\infty \le C_\zeta^2.$$

A bound for the second term on the right-hand side is more straightforward:

$$-2\tau\left\langle (d-1)\frac{f_0(R)R^{d-1}}{W^{n+1}r_h^{n+1}}\tilde{e}^{n+1}, \tilde{e}^{n+1}\right\rangle \le 2\tau DC_3\|\tilde{e}^{n+1}\|_2^2, \quad \text{with } d-1 \le D. \tag{6.19}$$

Meanwhile, an application of standard Cauchy inequality for the local truncation error term gives

$$\begin{aligned} 2\tau \left\langle \tau^3 l^* + h^4 g^*, \tilde{e}^{n+1} \right\rangle &\le \tau \|\tau^3 l^* + h^4 g^*\|_2^2 + \tau \|\tilde{e}^{n+1}\|_2^2 \\ &\le \tau C(\tau^3 + h^4)^2 + \tau \|\tilde{e}^{n+1}\|_2^2. \end{aligned} \tag{6.20}$$

Next, we provide a rough estimate for $\|D_h r_h^{n+1}\|_\infty$. A substitution of (6.16)-(6.20) into (6.15) yields

$$\begin{aligned} (\alpha_n - \tau(1 + C_1 + C_2 + 2DC_3))\|\tilde{e}^{n+1}\|_2^2 &\le (\alpha_n + \tau C_1)\|\tilde{e}^n\|_2^2 + \tau C_2 \|\widetilde{D}_h \tilde{e}^n\|_2^2 + \tau C(\tau^3 + h^4)^2 \\ &\le \tau \bar{C}(\tau^{\frac{7}{4}} + h^{\frac{5}{2}})^2, \end{aligned}$$

where $\bar{C}$ depends on C, C_1, C_2 and $\bar{C}_\alpha$. Subsequently, the following rough error estimate becomes available:

$$\|\tilde{e}^{n+1}\|_2 \le \widetilde{C} \tau^{\frac{1}{2}} (\tau^{\frac{7}{4}} + h^{\frac{5}{2}}),$$

with $\widetilde{C} := \left(\frac{\bar{C}}{C_\alpha/2}\right)^{\frac{1}{2}}$, if $\tau(1 + C_1 + C_2 + 2DC_3) \le C_\alpha/2$. By choosing $h = O(\tau)$, it is clear that

$$\|\tilde{e}^{n+1}\|_\infty \le \frac{C_m \|\tilde{e}^{n+1}\|_2}{h^{\frac{1}{2}}} \le C_m \widetilde{C} (\tau^{\frac{7}{4}} + h^{\frac{5}{2}}).$$

Then it follows that

$$\|D_h r_h^{n+1}\|_\infty = \|D_h W^{n+1} - D_h \tilde{e}^{n+1}\|_\infty \le C^* + C_m \widetilde{C} (\tau^{\frac{3}{4}} + h^{\frac{3}{2}}) \le C^* + 1 := C_0^*,$$

if $C_m \widetilde{C} (\tau^{\frac{3}{4}} + h^{\frac{3}{2}}) \le 1$.

In turn, the diffusion error estimate (6.17) could be refined as

$$2\tau \left\langle \frac{f_0(R) R^{d-1}}{D_h W^{n+1} D_h r_h^{n+1}} D_h \tilde{e}^{n+1}, D_h \tilde{e}^{n+1} \right\rangle_e \ge 2C_4 \tau \|D_h \tilde{e}^{n+1}\|_2^2, \tag{6.21}$$

with $C_4 := \frac{b_f}{C^* C_0^*}$. As a consequence, a substitution of (6.16)-(6.20) and (6.21) into (6.15) results in

$$\begin{aligned} &\alpha_n \|\tilde{e}^{n+1}\|_2^2 - \alpha_n \|\tilde{e}^n\|_2^2 + \tau C_4 \|D_h \tilde{e}^{n+1}\|_2^2 \\ &\le \tau \left(1 + \frac{C_2^2}{C_4} + C_1 + 2DC_3\right) \|\tilde{e}^{n+1}\|_2^2 + \tau C_1 \|\tilde{e}^n\|_2^2 + \tau C(\tau^3 + h^4)^2, \end{aligned}$$

where we have employed an obvious inequality $\|\widetilde{D}_h r_h^n\|_2 \le \|D_h r_h^n\|_2$, as well as the following estimate

$$\begin{aligned} &2\tau C_1 \|\tilde{e}^n\|_2 \cdot \|\tilde{e}^{n+1}\|_2 + 2\tau C_2 \|\widetilde{D}_h \tilde{e}^n\|_2 \cdot \|\tilde{e}^{n+1}\|_2 \\ &\le \tau C_1 \|\tilde{e}^n\|_2^2 + C_1 \tau \|\tilde{e}^{n+1}\|_2^2 + \frac{C_2^2 \tau}{C_4} \|\tilde{e}^{n+1}\|_2^2 + C_4 \tau \|\widetilde{D}_h \tilde{e}^n\|_2^2. \end{aligned}$$

Subsequently, a summation over time results in

$$\begin{aligned}
&\alpha_n\|\tilde{e}^{n+1}\|_2^2+\tau C_4\sum_{k=1}^{n+1}||\widetilde{D}_h\tilde{e}^k||_2^2\\
&\leq\tau\sum_{k=1}^{n}\frac{(\alpha_k-\alpha_{k-1})}{\tau}\|\tilde{e}^k\|_2^2+\tau\Big(\frac{C_2^2}{C_4}+1+C_1+2DC_3\Big)\sum_{k=1}^{n+1}\|\tilde{e}^k\|_2^2\\
&\quad+\tau C_1\sum_{k=1}^{n}\|\tilde{e}^k\|_2^2+CT(\tau^3+h^4)^2,
\end{aligned}$$

$$\|\tilde{e}^{n+1}\|_2^2+\tau\frac{C_4}{C_\alpha}\sum_{k=1}^{n+1}||\widetilde{D}_h\tilde{e}^k||_2^2\leq\frac{\tau}{C_\alpha}(\frac{C_2^2}{C_4}+1+2C_1+2DC_3+\widetilde{C}_\alpha)\sum_{k=1}^{n+1}\|\tilde{e}^k\|_2^2+\frac{CT}{C_\alpha}(\tau^3+h^4)^2,$$

where the following estimate has been utilized

$$\begin{aligned}
\Big\|\frac{\alpha^k-\alpha^{k-1}}{\tau}\Big\|_\infty&=\Big\|\frac{f_0(R)R^{d-1}}{m[f_0(R)R^{d-1}]^{m-1}}\cdot\frac{\big((r_h^k)^{d-1}\widetilde{D}_hr_h^k\big)^{m-1}-\big((r_h^{k-1})^{d-1}\widetilde{D}_hr_h^{k-1}\big)^{m-1}}{\tau}\Big\|_\infty\\
&=\Big\|\frac{f_0(R)R^{d-1}}{m[f_0(R)R^{d-1}]^{m-1}}(m-1)((\vartheta)^{d-1}\widetilde{D}_h\vartheta)^{m-2}(d-1)(\vartheta)^{d-2}\widetilde{D}_h\vartheta\frac{r_h^k-r_h^{k-1}}{\tau}\Big\|_\infty\\
&+\Big\|\frac{f_0(R)R^{d-1}}{m[f_0(R)R^{d-1}]^{m-1}}(m-1)((\vartheta)^{d-1}\widetilde{D}_h\vartheta)^{m-2}(\vartheta)^{d-1}\frac{\widetilde{D}_hr_h^k-\widetilde{D}_hr_h^{k-1}}{\tau}\Big\|_\infty\\
&\leq\frac{B_f}{mb_f^{m-1}}[C_\vartheta^1(C_t^*+1)+C_\vartheta^2(\tilde{C}_t^*+1)]:=\widetilde{C}_\alpha.
\end{aligned}$$

In particular, we notice that $[0,T]$ is the time interval, (6.12) and (6.13) are utilized, with ϑ lying between r_h^k and r_h^{k-1}, and

$$\|(m-1)((\vartheta)^{d-1}\widetilde{D}_h\vartheta)^{m-2}(d-1)(\vartheta)^{d-2}\widetilde{D}_h\vartheta\|_\infty\leq C_\vartheta^1,$$

$$\|(m-1)((\vartheta)^{d-1}\widetilde{D}_h\vartheta)^{m-2}(\vartheta)^{d-1}\|_\infty\leq C_\vartheta^2.$$

Subsequently, an application of the discrete Gronwall inequality results in

$$\|\tilde{e}^{n+1}\|_2^2+\tau\frac{C_4}{C_\alpha}\sum_{k=1}^{n+1}||\widetilde{D}_h\tilde{e}^k||_2^2\leq\mathrm{e}^{C_0T}\frac{CT}{C_\alpha}(\tau^3+h^4)^2,\quad\text{i.e., }\|\tilde{e}^{n+1}\|_2\leq\gamma(\tau^3+h^4),$$

where $C_0:=\frac{1}{C_\alpha}(\frac{C_2^2}{C_4}+\widetilde{C}_\alpha+1+2C_1+2DC_3)$ and $\gamma:=\Big(\frac{CT}{C_\alpha}\Big)^{\frac{1}{2}}\mathrm{e}^{\frac{C_0T}{2}}$.

Therefore, the a-priori assumption (6.6) also becomes available at t^{n+1}:

$$\|\tilde{e}^{n+1}\|_2\leq\gamma(\tau^3+h^4)\leq\tau^{\frac{11}{4}}+h^{\frac{7}{2}},$$

where $\tau\leq\gamma^{-4}$, $h\leq\gamma^{-2}$.

On the other hand, based on the fact that

$$\|D_h\tilde{e}^{n+1}\|_2 = \|D_h r_h^{n+1} - D_h W^{n+1}\|_2 \le C\gamma(\tau^2 + h^3),$$

we obtain

$$\|r_h^{n+1} - r_e^{n+1}\|_2 \le C(\tau + h^2),$$

and

$$\|D_h r_h^{n+1} - D_h r_e^{n+1}\|_2 \le C(\tau + h^2).$$

Finally, we assess the error between the numerical solution f_h^{n+1} and the exact solution f_e^{n+1}

$$\begin{aligned}
&\|f_e^{n+1} - f_h^{n+1}\|_2 = \left\| \frac{f_0(R)R^{d-1}}{(r_e^{n+1})^{d-1}\partial_R r_e^{n+1}} - \frac{f_0(R)R^{d-1}}{(r_h^{n+1})^{d-1}\widetilde{D}_h r_h^{n+1}} \right\|_2 \\
&\le \left\| \frac{f_0(R)R^{d-1}}{(r_e^{n+1})^{d-1}\partial_R r_e^{n+1}} - \frac{f_0(R)R^{d-1}}{(r_e^{n+1})^{d-1}\widetilde{D}_h r_e^{n+1}} \right\|_2 + \left\| \frac{f_0(R)R^{d-1}}{(r_e^{n+1})^{d-1}\widetilde{D}_h r_e^{n+1}} - \frac{f_0(R)R^{d-1}}{(r_e^{n+1})^{d-1}\widetilde{D}_h r_h^{n+1}} \right\|_2 \\
&+ \left\| \frac{f_0(R)R^{d-1}}{(r_e^{n+1})^{d-1}\widetilde{D}_h r_h^{n+1}} - \frac{f_0(R)R^{d-1}}{(r_h^{n+1})^{d-1}\widetilde{D}_h r_h^{n+1}} \right\|_2 \\
&\le C(\tau + h^2).
\end{aligned}$$

□

References

1. F. Andreu, V. Caselles, J. M. Mazón, J. Soler, and M. Verbeni, Radially Symmetric Solutions of a Tempered Diffusion Equation. A Porous Media, Flux-Limited Case, SIAM J. Math. Anal., 44 (2), 1019-1049 (2012).
2. S. B. Angenent and D. G. Aronson, The focusing problem for the radially symmetric porous medium equation, Commun. Partial. Differ. Equ., 20 (7-8), 1217-1240 (1995).
3. D. G. Aronson, Regularity properties of flows through porous media, SIAM J. Appl. Math., 17, 461–467 (1969).
4. G. I. Barenblatt, On some unsteady motions of a liquid or a gas in a porous medium, Prikl. Mat. Meh., 16 (1), 67–78 (1952) (in Russian).
5. A. Bressan, G. Q. G. Chen, M. Lewicka, and D. Wang, Nonlinear Conservation Laws and Applications, Springer (2011).
6. J. A. Carrillo, S. Hittmeir, B. Volzone, and Y. Yao, Nonlinear aggregation-diffusion equations: radial symmetry and long time asymptotics, Invent. Math., 218, 889-977 (2019).
7. W. Chen, S. Conde, C. Wang, X. Wang and S. M. Wise, A linear energy stable scheme for a thin film model without slope selection, J. Sci. Comput., 52 (3), 546–562 (2012).
8. W. Chen, Y. Liu, X. Wang and S. M. Wise, Convergence analysis of a fully discrete finite difference scheme for Cahn-Hilliard-Hele-Shaw equation, Math. Comput., 85 (301), 2231–2257 (2016).
9. J. V. L. Chew, J. Sulaiman and A. Sunarto, Numerical Approximation to Porous Medium Equation Using a Quarter-Sweep Based Finite Difference and Explicit Four-Points Group, Procedia Comput., 227, 849-857 (2023).
10. E. DiBenedetto and D. Hoff, An interface tracking algorithm for the porous medium equation, Trans. Am. Math. Soc., 284, 463–500 (1984).
11. C. Duan, C. Liu, C. Wang and X. Yue, Numerical complete solution for random genetic drift by Energetic Variational approach, ESAIM: Math. Model. Num., 53 (2), 615-634 (2019).
12. C. Duan, C. Liu, C. Wang and X. Yue, Numerical methods for porous medium equation by an energetic variational approach, J. Comput. Phys., 385, 13-32 (2019).

13. C. Duan, C. Liu, C. Wang and X. Yue, Convergence analysis of a numerical scheme for the porous medium equation by an energetic variational approach, Numer. Math. Theor. Meth. Appl., 13 (1), 63-80 (2020).
14. C. Duan, W. Chen, C. Liu, C. Wang and X. Yue, A second order accurate numerical scheme for the porous medium equation by an energetic variational approach, Commu. Math. Sci., 20 (4), 987-1024 (2022).
15. C. Duan, W. Chen, C. Liu, X. Yue and S. Zhou, Structure-preserving numerical methods for nonlinear Fokker–Planck equations with nonlocal interactions by an energetic variational approach, SIAM J. Sci. Comput., 43 (1), B82-B107 (2021).
16. C. Duan, W. Chen, C. Liu, C. Wang and S. Zhou, Convergence analysis of structure-preserving numerical methods for nonlinear Fokker–Planck equations with nonlocal interactions, Math. Methods Appl. Sci., 45 (7), 3764–3781 (2022).
17. W. E and J. Liu, Projection method I: convergence and numerical boundary layers, SIAM J. Numer. Anal., 32, 1017–1057 (1995).
18. D. J. Eyre, Unconditionally gradient stable time marching the Cahn-Hilliard equation, MRS online proceedings library, 529, 39 (1998).
19. B. H. Gilding and J. Goncerzewicz, Localization of Solutions of Exterior Domain Problems for the Porous Media Equation with Radial Symmetry, SIAM J. Math. Anal., 31 (4), 862-893 (2000).
20. J. Gratton and C. Vigo, Evolution of self-similarity, and other properties of waiting-time solutions of the porous medium equation: the case of viscous gravity currents, J. Appl. Math., 9, 327–350 (1998).
21. J. L. Graveleau and P. Jamet, A finite difference approach to some degenerate nonlinear parabolic equations, SIAM J. Appl. Math., 20, 199–223 (1971).
22. M. Hayek, An exact solution for a nonlinear diffusion equation in a radially symmetric inhomogeneous medium, Comput. Math. Appl., 68 (12), 1751-1757 (2014).
23. G. E. Hernandez and I. M. Roussos, The Hölder Exponent for Radially Symmetric Solutions of Porous Medium Type Equations, Can. J. Math., 43 (2), 313-321 (1991).
24. Z. Hu, C. Liu, Y. Wang and Z. Xu, Energetic variational neural network discretizations ofgradient ffows, SIAM J. Sci. Comput., 46 (4), A2528-A2556 (2024).
25. Y. Hyon, D. Y. Kwak and C. Liu, Energetic variational approach in complex fluids: maximum dissipation principle, Discrete Contin. Dyn. Syst., 26 (4), 1291–1304 (2010).
26. A. S. Kalašnikov, Formation of singularities in solutions of the equation of nonstationary filtration, Ž. Vycisl. M̆at. Mat. Fiz., 7, 440–444 (1967).
27. W. Lee, L. Wang and W. Li, Deep JKO: Time-implicit particle methods for general nonlinear gradient flows, J. Comput. Phys., 514, 113187 (2024).
28. L. S. Leibenzon, The motion of a gas in a porous medium, in: Complete Works, vol. 2, Acad. Sciences URSS, Moscow (1953).
29. C. Liu and J. Shen, A phase field model for the mixture of two incompressible fluids and its approximation by a Fourier-spectral method, Physica D, 179 (3–4), 211–228 (2003).
30. C. Liu and H. Wu, An energetic variational approach for the Cahn-Hilliard equation with dynamic boundary conditions, Arch. Ration. Mech. Anal., 233 (1), 167-247 (2019).
31. C. Liu and Y. Wang, On Lagrangian schemes for porous medium type generalized diffusion equations: A discrete energetic variational approach, J. Comput. Phys., 417, 109566 (2020).
32. C. Liu, C. Wang, S. M. Wise, X. Yue, and S. Zhou, A second order accurate, positivity preserving numerical method for the Poisson–Nernst–Planck system and its convergence analysis, J. Sci. Comput., 97 (1), 23 (2023).
33. C. Liu, J. E. Sulzbach and Y. Wang, Non-isothermal diffuse interface model for phase transition and interface evolution, SIAM J. Appl. Math., 85 (6), 2611-2635 (2025).
34. Q. Liu, C. Duan and W. Chen, EnVarA-FEM for the flux-limited porous medium equation, J. Comput. Phys., 493, 112432 (2023).
35. Y. Nesterov and A. Nemirovskii, Interior-Point Polynomial Algorithms in Convex Programming, SIAM (1994).
36. C. Ngo and W. Z. Huang, A study on moving mesh finite element solution of the porous medium equation, J. Comput. Phys., 331, 357–380 (2017).
37. O. A. Oleĭnik, A. S. Kalašnikov and Y. Čžou, The Cauchy problem and boundary problems for equations of the type of non-stationary filtration, Izv. Akad. Nauk SSSR, Ser. Mat., 22, 667–704 (1958).
38. O. A. Oleĭnik and E.V. Radkevič, Second-order equations with nonnegative characteristic form, Amer. Math. Soc. (1973).

39. L. Onsager, Reciprocal relations in irreversible processes, II. Phys. Rev., 38, 2265-2279 (1931).
40. L. Onsager, Reciprocal relations in irreversible processes, I, Phys. Rev., 37 (4), 405 (1931).
41. M. S. Park, C. Kim, H. Son and H. J. Hwang, The deep minimizing movement scheme, J. Comput. Phys., 494, 112518 (2023).
42. S. I. Shmarev, Interfaces in multidimensional diffusion equations with absorption terms, Nonlinear Anal., 53, 791–828 (2003).
43. J. W. Strutt, Some general theorems relating to vibrations, Proc. Lond. Math. Soc. IV, 357–368 (1873).
44. J. L. Vázquez, The Porous Medium Equation, Oxford University Press, Oxford (2007).
45. C. Wang and S. M. Wise, An energy stable and convergent finite-difference scheme for the modified phase field crystal equation, SIAM J. Numer. Anal., 49 (3), 945–963 (2011).
46. M. Westdickenberg and J. Wilkening, Variational particle schemes for the porous medium equation and for the system of isentropic Euler equations, ESAIM: M2AN, 44 (1), 133–166 (2010).
47. S. S. Zaman, R. Amin, N. Haider, A. Aloqaily and N. Mlaiki, Haar wavelet collocation technique for numerical solution of porous media equations, Commun. Partial. Differ. Equ., 10, 100728 (2024).
48. Q. Zhang and Z. L. Wu, Numerical simulation for porous medium equation by local discontinuous Galerkin finite element method, J. Sci. Comput., 38 (2), 127–148 (2009).